Contents lists available at ScienceDirect

Remote Sensing of Environment

Comparing the relationship between NDVI and SAR backscatter across different frequency bands in agricultural areas

Thomas Roßberg *, Michael Schmitt

University of the Bundeswehr Munich, Werner-Heisenberg-Weg 39, 85577, Neubiberg, Germany

ABSTRACT

The objective of this study is to investigate the relationship between the Normalized Difference Vegetation Index (NDVI) and Synthetic Aperture Radar (SAR) data at multiple frequencies, focusing on S- and C-band data with additional analysis for X- and L-band. This is the foundation for the translation of SAR data into NDVI values, thereby enabling the filling of gaps in NDVI data due to cloud cover. This study encompasses three distinct study areas in Argentina, Australia, and Vietnam, which exhibit considerable climatic and agricultural differences. NovaSAR-1 S-band and Sentinel-1 C-band data were acquired for all areas, with the addition of COSMO-SkyMed X-band and SAOCOM L-band SAR data for one region. Following the processing of the SAR data and the derivation of NDVI values from optical Sentinel-2 data, the relationship between them is analyzed for field-wise aggregated data.

The relationship between S- and C-band SAR data and NDVI values is observed to be strong for all fields. Consequently, cross-polarized (HV or VH) data demonstrated this relationship for all fields with a Pearson correlation coefficient $\rho > 0.5$, whereas for co-polarized data (HH or VV), this could only be shown for some fields and crops. In the case of rice paddy fields, however, a different relationship is observed. While both S- and C-band data demonstrate a good relationship, this is primarily evident in the case of co-polarized data, with cross-polarized data exhibiting a comparatively weaker relationship. A relationship was observed for X-band data, but no relationship could be attested for L-band data. Neither the cross-ratio nor the radar vegetation index (RVI) generally showed a stronger relationship with the NDVI compared to a single polarization.

The demonstrated relationship between NDVI values and SAR backscatter data allows for a translation to be feasible. Consequently, the planned launch of the NISAR satellite, comprising S- and L-band SAR sensors, will facilitate new opportunities for agricultural monitoring. However, the retrieval of NDVI values from SAR data is a complex topic, as numerous factors, including crop type, crop phenology, SAR geometry and frequency, and others, influence this relationship.

1. Introduction

Agriculture provides food for humans and animals alike and therefore is of utmost importance. The importance of monitoring agricultural fields and landscapes is driven by the need to estimate yields and anticipate food insecurity (Weiss et al., 2020) or observe the occurrence and spread of pests and diseases (Zhang et al., 2019). A variety of sensor types are employed for agricultural monitoring, with multispectral optical and synthetic aperture radar (SAR) sensors representing the primary focus. Although there has been a greater focus on optical sensors, their primary limitation—the lack of data due to cloud coverage and reliance on solar illumination—has hindered their adoption, particularly in tropical regions. In contrast, synthetic aperture radar (SAR) data offers significant advantages, including the ability to acquire images in all weather conditions and at any time of day or night. Nevertheless, the adoption of SAR data for agricultural monitoring is relatively slow, due to several factors, including the lower resolution of freely available data, the greater difficulty of visual interpretation, and the lack of historical data for comparison.

Vegetation indices (VIs) are a common tool in the analysis of optical data due to their ease of use, which allows for the integration of information from multiple spectral bands into a single value. In the context of vegetation, the normalized difference vegetation index (NDVI) is the most popular one. The NDVI is a measure of vegetation greenness (Chuvieco, 2020), which can be used as a rough indicator of crop state. One potential solution to this challenge is to translate the SAR data into NDVI values, which relies on a relationship between the two modalities. This approach offers a means of combining the advantages of the SAR sensor's all-weather imaging capability with

---

the ease of interpretation of vegetation indices. For C-band data, a relationship between the two modalities was demonstrated, as well as the successful estimation of NDVI from SAR data. However, for S-band data, neither of these outcomes has yet been shown and for X- and L-band, this was also not exhaustively studied. The planned launch of NASA-ISRO Synthetic Aperture Radar (NISAR) in 2024, which will include S- and L-band SAR sensors, makes further investigation into this area highly valuable.

1.1. Related research

This paper examines the relationship between SAR backscatter and NDVI values. In this regard, existing research on this relationship is relevant, as are approaches to estimating NDVI values from SAR data, given that this process necessarily entails a relationship.

The relationship between L-, X-, and especially C-band SAR data and optical vegetation indices or crop parameters has been explored in numerous studies. Thereby, the choice of SAR frequencies investigated in each study is influenced by two primary factors: the optimal wavelength and the availability of data for that specific wavelength. The chosen wavelength is crucial as it determines the penetration depth into the crop canopy and also determines, which parts of the vegetation contribute to the radar response, because backscattering only occurs for objects of a similar or larger size than the radar wavelength (Rosenqvist and Killough, 2018). For instance, short X-band waves with a 3 cm wavelength interact already with the topmost leaves of the vegetation and therefore the waves do not penetrate deeply into canopy. In contrast, L-band waves with a 20 cm wavelength do not interact so strongly with small leaves, but more with larger structures like stalks and therefore they can penetrate the whole crop volume even for tall crops like Maize.

Very little research was carried out so far investigating S-band SAR data for different applications like vegetation monitoring, because only a limited number of S-band SAR systems were deployed so far. Only recently has there been an increase in research utilizing this frequency, following the launch of NovaSAR-1 and in anticipation of the launch of NISAR, which will have both S- and L-band SAR sensors. Nevertheless, no studies have yet been conducted that establish a link between NDVI and S-band backscatter data.

In contrast, numerous publications examine the relationship between X-, C-, and L-band SAR data and crop and plant parameters, as well as optical vegetation indices, due to the availability of a multitude of sensors. For C-band, a relationship between NDVI values and SAR backscatter has been demonstrated for maize (Alvarez-Mozos et al., 2021), barley, wheat, grassland, and maize (Holtgrave et al., 2020), or canola (Jiao et al., 2021). Moreover, the biomass of corn could be estimated with both SAR and optical data (Hosseini et al., 2019), and the same was possible for wheat with both C- and L-band data (Hosseini and McNairn, 2017). Additionally, time series of Sentinel-1's interferometric coherence and the NDVI are well related (Villarroya-Carpio et al., 2022). Similar to C-band, X-band SAR data is related to the height, biomass, and water content of maize (Baup et al., 2016)) or to the NDVI values of carrot fields (Segalini et al., 2014). In the second study, the authors note a strong dependence of the field orientation with respect to the SAR sensor. Furthermore, the leaf area index and plant height of sunflowers have been demonstrated to be related to SAR backscatter data of X-, C-, and L-band frequencies (Fieuzal and Baup, 2016). Similarly, a relationship between the same three frequencies and NDVI values has been observed in meadows (Wang et al., 2013). The aforementioned studies collectively demonstrate the existence of a relationship between SAR data and vegetation indices.

The successful estimation of VI values from SAR data provides further evidence that a relationship exists between the two sets of data. Consequently, both machine learning techniques, such as random forests, and deep learning techniques, including convolutional neural networks, are employed. The estimation of NDVI from C-band SAR

backscatter has been demonstrated for small areas in several studies (Scarpa et al., 2018; Filgueiras et al., 2019; de Castro et al., 2024). Both NDVI and enhanced vegetation index (EVI) are estimated for a larger study area (dos Santos et al., 2022), and the global applicability to retrieve NDVI values from single-date SAR images has also been demonstrated (Roßberg and Schmitt, 2023). Collectively, these studies underscore the relationship between C-band SAR data and NDVI.

1.2. Contributions

This study makes two significant contributions to the field. It is the first to analyze the relationship between NDVI values and S-Band SAR backscatter. Additionally, it is unique in that SAR backscatter and NDVI values are related to each other for multiple SAR frequencies and multiple study areas, thereby providing more comprehensive insights into the spatial applicability and performance of SAR-based vegetation monitoring.

2. Data

For this study, three diverse areas were selected with varying climates and agricultural practices (Section 2.1), for which SAR and optical data are acquired (Sections 2.2 and 2.3) and field outlines extracted (Section 2.4).

2.1. Study areas

To gain a broad understanding of the relationship between SAR backscatter and NDVI values, three different areas with distinct climates and agricultural practices were selected: near the cities of Bell Ville in Argentina and Boort in Australia, and an area in the Mekong River Delta in Vietnam. Their location on the globe is shown in Fig. 1(a). The choice of study areas was limited due to the limited availability of suitable S-band NovaSAR-1 data. Nevertheless, these three regions offer a variety of climates and crop types, providing a robust basis for analysis. Mainly Sentinel-1 C-band and NovaSAR-1 S-band data are used, but for one study area COSMO-SkyMed X-band and SAOCOM L-band data are also used. The study areas are described in detail in the following sections.

2.1.1. Bell Ville (Argentina)

Bell Ville, located in Argentina, experiences a monsoon-influenced humid subtropical climate (Köppen-Geiger classification: Cwa) with an average temperature of 17.4 °C and 952 mm of annual precipitation. The region has mild winters from June to August with temperatures of 10 to 12 °C and minimal precipitation (13–17 mm/month), and hot summers from December to February with average temperatures of 23–24 °C and significant precipitation (120–160 mm/month). In the Union Department, whose capital is Bell Ville, soy (46%), corn (29%), and wheat (16%) are the main crops (Dirección de Estimaciones Agrícolas, 2023). The agricultural season runs from November to May, with soy planted from mid-November to mid-January, corn from mid-September to November, and wheat from mid-May to July, with corresponding harvest seasons of mid-March to mid-June for soy and corn, and mid-November to mid-January for wheat (U.S. Department of Agriculture, 2024). The region is relatively flat, with elevations ranging from 115 m to 140 m.

Six NovaSAR-1 acquisitions were selected for further analysis. They are acquired in the 20 m ScanSAR mode with two polarizations, HH and HV, and have an angle of incidence between 22° and 31°. They are provided by CSIRO in ScanSAR detected (SCD) format. The corresponding Sentinel-1 and −2 images are usually acquired within three days of the NovaSAR-1 acquisition, with two exceptions, where Sentinel-1 data are acquired four and six days before the NovaSAR-1 one. All scenes were acquired between December 2023 and April 2024, the main growing season for this area. The exact acquisition times of all three sensors together with the incidence angle are given in Table 1.

Table 1

Overview of the acquisition dates of the three sensors utilized for the Bell Ville study area in Argentina. The incidence angle is given for the SAR data.

NovaSAR-1		Sentinel-1		Sentinel-2
date	angle	date	angle	date
2023-12-24	27°–30°	2023-12-20	35°–37°	2023-12-25
2024-01-02	29°–31°	2024-01-01	35°–37°	2024-01-04
2024-01-19	24°–27°	2024-01-13	35°–37°	2024-01-19
2024-02-16	29°–30°	2024-02-18	35°–37°	2024-02-13
2024-03-03	22°–24°	2024-03-01	35°–37°	2024-03-04
2024-03-25	24°–27°	2024-03-25	35°–37°	2024-03-24

Table 2

Overview of the used SAR and optical scenes used for the Boort study area in Australia. The incidence angle of each scene is given for both NovaSAR-1 and Sentinel-1. Additionally, the ScanSAR mode resolution of each NovaSAR-1 scene is listed.

NovaSAR-1			Sentinel-1		Sentinel-2
date	resolution	angle	date	angle	date
2021-08-07	35 m	15°–22°	2021-08-06	34°–38°	2021-08-08
2022-01-20	30 m	24°–29°	2022-01-21	34°–38°	2022-01-20
2022-06-01	35 m	15°–22°	2022-06-02	34°–38°	2022-06-04

2.1.2. Boort (Australia)

Boort, located in Australia, is characterized by a cold semi-arid climate (BSk of the Köppen-Geiger classification) with an average annual temperature of 15.6 °C and 371 mm of precipitation. The climate features warm summers from December to February with average temperatures ranging from 20–22 °C and low precipitation (20 mm/month), and cooler winters from June to August with temperatures around 8–9 °C and higher precipitation (40 mm/month) (Karger et al., 2017, 2021).

The region's elevation varies from 60 m to 110 m, with mild elevation changes and slopes of less than 1°. The primary crops include wheat (42%), barley (25%), and canola (17%), as well as pasture (13.2%) (Australian Bureau of Statistics, 2024). Wheat and barley are typically planted from April to June and harvested between October and January, while canola is planted in April and harvested from mid-October (U.S. Department of Agriculture, Foreign Agricultural Service, International Production Assessment Division, 2021).

Three NovaSAR-1 acquisitions were selected for this area, two during the winter growing season (2021-08-07 and 2022-06-01) and a third on 2022-01-20 during the drier summer without much green vegetation. All three images were acquired in ScanSAR mode with three polarizations VV, HH, and HV. They have slightly different resolutions of 35 m and 30 m for the summer and winter acquisitions, respectively, and also different incidence angles ranging from 15.1° to 28.5°, as they were acquired from different orbits. For this area, CSIRO provided analysis-ready data (ARD) with radiometric terrain correction, which we used. The optical and Sentinel-1 C-band SAR images are acquired on approximately the same days as the NovaSAR-1 data, with a maximum difference of three days. The exact acquisition dates of all three sensors, together with the incidence angles and, for NovaSAR-1, the ScanSAR mode resolution used, are detailed in Table 2.

2.1.3. Mekong River Delta (Vietnam)

The third study area is located in the Mekong River Delta in southern Vietnam in the province of Đồng Tháp. It is almost entirely covered with rice fields, as the Mekong Delta produces 56% of Vietnam's rice (U.S. Department of Agriculture, Foreign Agricultural Service, International Production Assessment Division, 2017). The terrain is extremely flat, with elevations ranging from 0 m to 10 m above sea level. The climate of the region is predominantly monsoonal (Köppen-Geiger classification As and Aw), with an average annual precipitation of 1600 mm. The rainy season occurs from May to November, with more than 150 mm of rain per month, while the dry season from December

to April has less than 50 mm of rain per month. Temperatures remain fairly constant throughout the year, ranging from 26–29 °C. Rice is cultivated up to three times per year, with our study period covering the summer–autumn (July 1 to January 31) and autumn–winter (March 1 to August 31) seasons (Clauss et al., 2018).

Two dates were chosen in March and August 2023. For these dates, SAR data could be acquired at four frequencies: NovaSAR-1 S-band, SAOCOM L-band, Sentinel-1 C-band, and COSMO-SkyMed Second Generation (CSG) X-band data. Only CSG data could not be acquired on both dates, but only for August 2023. Data from all sensors are acquired no more than three days apart from the Sentinel-2 optical acquisition. For Sentinel-1, both ascending and descending orbits could be used. Similarly, two SAOCOM acquisitions were available in August 2023.

The NovaSAR-1 data are acquired in 20 m resolution dual-polarized ScanSAR mode with HH and HV polarization and are provided by CSIRO in SCD format. The orbit state and position are inaccurate for the acquisition on 2023-08-06, resulting in a geolocation error of several kilometers, which was manually corrected after data processing. This leads to small errors in the backscatter, as the angle of incidence is off by 0.2°, as well as errors where the terrain is not flat. Since most of the terrain is very flat, this does not affect the data analysis and results. SAOCOM and CSG data were acquired in stripmap mode with HH and HV polarization, Sentinel-1 in IW mode. All three SAOCOM acquisitions were not perfectly geolocated but were off by 10 m to 50 m, which was corrected manually.

For all five sensors, the exact acquisition dates as well as the incidence angles of the SAR scenes are given in Table 3.

2.2. SAR data

This study utilizes SAR data from multiple sensors with different frequencies and imaging modes.

NovaSAR-1 is a space-borne S-band SAR system launched in 2018 and operated by a consortium of various space agencies and partners (Held et al., 2019). Australia's Commonwealth Scientific and Industrial Research Organisation (CSIRO) provides data free of charge on their data portal.[1]

Sentinel-1 is a global monitoring mission by the European Space Agency (ESA) utilizing C-band SAR to provide continuous data of the Earth's surface (Torres et al., 2012). The Sentinel-1 data used in this study were captured in interferometric wide swath (IW) mode with VV and VH polarizations with a raw resolution of 3×22 m (Rg × Az). The Level-1 Ground Range Detected (GRD) data were downloaded from the Copernicus Browser data platform,[2] which are already detected, multi-looked, and projected to ground range.

The Argentine SAOCOM 1 A and 1B satellites are part of the L-band SAR constellation, which is overseen by the National Space Activities Commission (CONAE). This study uses Single Look Complex (SLC) data from SAOCOM in Stripmap mode. The data utilized in this study is taken in dual-polarized stripmap mode with a ground resolution of 10 m $\times 5$ m (Rg × Az) and includes HH and HV polarizations.

The fourth sensor used is from the second-generation COSMO-SkyMed (CSG) satellite constellation, which carries X-band SAR systems and is operated by the Italian Space Agency (ASI). Images are taken in dual-polarized (HH and HV) stripmap mode with a resolution of 3×3 m. The data are provided in the Level-1B format, which is already focused, amplitude-detected, radiometrically equalized, and represented in ground projection.

An overview of the data from all sensors including the imaging mode and data product for each study area is provided in Table 4. Upon visualizing an example image of each SAR sensor the resolution differences of the sensors become evident. CSG and SAOCOM demonstrate

---

[1] https://data.novasar.csiro.au/

[2] https://browser.dataspace.copernicus.eu/

Table 3

Overview of the acquisition dates for the Mekong River Delta study area in Vietnam along with the incidence angle for all SAR scenes.
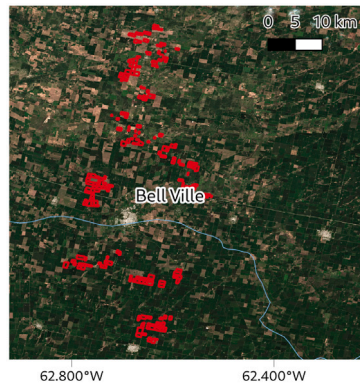
| NovaSAR		Sentinel-1		SAOCOM		CSG		Sentinel-2
date	angle	date	angle	date	angle	date	angle	date
2023-03-05	25–27°	2023-03-05	38°–41°	2023-03-03	21°–23°			2023-03-06
		2023-03-06	40°–43°	2023-03-06	29°–31°			
2023-08-08	13–15°	2023-08-08	38°–41°	2023-08-05	29°–31°	2023-08-06	44°–46°	2023-08-08
		2023-08-09	40°–43°					
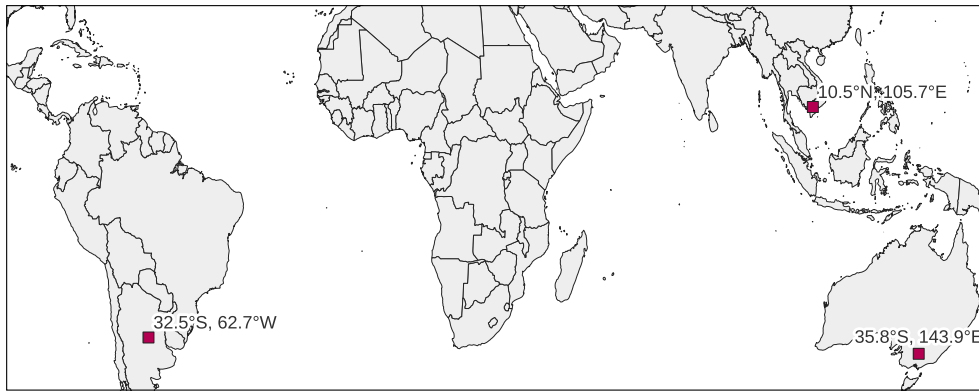
(a) Location of the three study regions on the Earth.
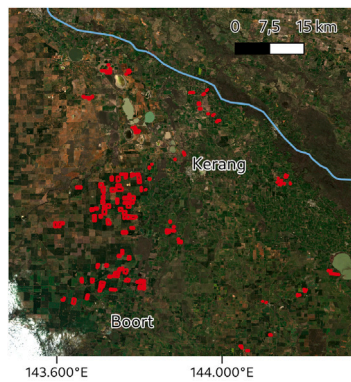
(b) Boort (Australia), 2021-08-08

(c) Bell Ville (Argentina), 2024-01-19
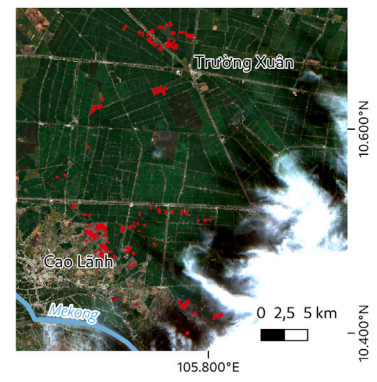
(d) Mekong Delta (Vietnam), 2023-03-06

Fig. 1. Overview of the three study areas with their location (1(a)) and a Sentinel-2 RGB visualization overlaid with the field outlines (1(b),1(c),1(d)).

Table 4

Overview of SAR sensors utilized in this study, along with their imaging parameters and data availability for each of the three study areas Boort (B), Bell Ville (BV), and Mekong River Delta (MRD).

Sensor	Band	Fre-quency (GHz)	Wave-length (cm)	Image mode	Polarization	Resolution (Rg × Az) (m × m)	Data product	Pixel spacing (m × m)	Study region		
									B	BV	MRD
NovaSAR-1	S	3.200	9.4 cm	ScanSAR	HH,HV,VV	30 × 30, 35 × 35	ARD	22.3 × 22.3	x	–	–
NovaSAR-1	S	3.200	9.4 cm	ScanSAR	HH,HV	20 × 20	CSD	10 × 10	–	x	x
Sentinel-1	C	5.405	5.5 cm	IW	VH,VV	20 × 22	GRD	10 × 10	x	x	x
SAOCOM	L	1.275	23.5 cm	Stripmap	HH,HV	3.75 × 3.23	L1A	2.4 × 6.95	–	–	x
CSG	X	9.600	3.1 cm	Stripmap	HH,HV	3 × 3	DGM_B	1.25 × 1.25	–	–	x

superior resolution compared to Sentinel-1, which still exhibits a better resolution compared to NovaSAR-1 data. For each sensor, the data over the Mekong River Delta of a single date together with a zoomed-in detail view is displayed in Fig. 2.

2.3. Optical data

The optical data utilized in this study is from Sentinel-2, a global monitoring mission by the European Space Agency (ESA) and provides multispectral imagery with a 10 m resolution. Captured spectral data includes visible, near-infrared, and shortwave infrared light with wavelengths from 443 nm to 2200 nm. Surface reflectance data (Level-2A) are used in this study, which are processed using Sen2Cor by ESA. In addition to providing surface reflectance data free from atmospheric effects, Sen2Cor also generates a scene classification layer (SCL) that annotates, among other things, cirrus and other clouds, their shadows, and water surfaces. An example visualization of the optical data for each study area is given in Figs. 1(b)–1(d).

(a) Sentinel-1, 2024-08-09   (b) NovaSAR, 2023-08-06   (c) CSG, 2023-08-06   (d) SAOCOM, 2023-08-05
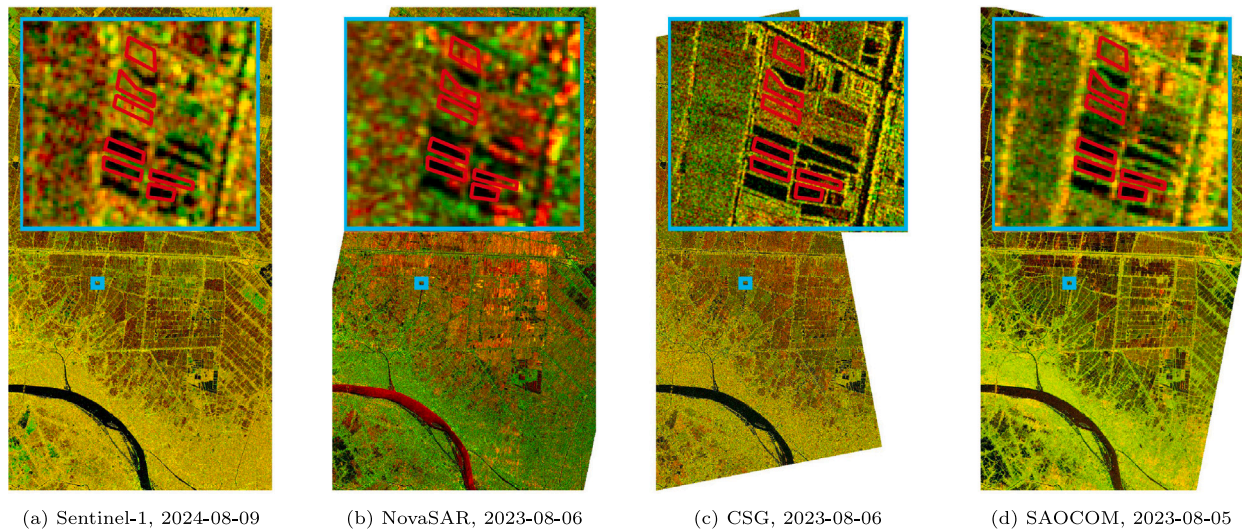
Fig. 2. Visualization of the SAR data for the Mekong River Delta study area. A zoomed-in detail view is shown to illustrate the different image resolutions. The polarizations of each image are displayed in the red and green channels of the image, and the acquisition date is given for each image. (For interpretation of the references to color in this figure legend, the reader is referred to the web version of this article.)

2.4. Field outlines

The outlines of the agricultural fields in all three study regions were delineated manually using data from the Sentinel-2 satellite as well as Google aerial imagery. It was ascertained that all fields exhibit a uniform NDVI across all dates, as well as a homogeneous appearance in the SAR imagery. To avoid mixed pixels at the field boundaries, all polygons are designed to remain entirely within the field edges, with a buffer zone around the edge.

In total, around 200 fields were delineated for each of the three study areas. The Boort study area encompasses 174 fields, the Bell Ville area 204, and the Mekong River Delta region 208. Because of different agricultural practices, the field sizes change substantially between the study regions: Both Boort and Bell Ville feature larger fields with a median size of 16.4 hectares and 30 hectares, respectively. In the case of Boort, one-third of the fields are less than 10 hectares in size, another third are between 10 and 40 hectares, and the remainder are up to 120 hectares in size. In the Bell Ville area, field sizes are more homogeneous, with 60% of fields measuring between 10 and 40 hectares. In contrast, the fields in the Mekong River Delta are relatively small, with 85% of them being smaller than 2 hectares and almost all of them being smaller than 4 hectares. For all three regions, the labeled polygons are shown in Fig. 1, superimposed on the Sentinel-2 RGB image.

2.5. Crop classification

The relationship between NDVI and SAR backscatter is distinct for different crops (Villarroya-Carpio and Lopez-Sanchez, 2023). Therefore, the relationship should be investigating separately per crop, which requires a crop type map.

For the Bell Ville study area, the National Map of Crops 2023/24 is used (de Abelleyra et al., 2024), which is depicted for the study area in Fig. 3. For this crop map, features derived from Landsat and Sentinel-2 imagery are used to train a random forest classifier using samples taken at field surveys. An overall accuracy of 0.91 is reported for the region Bell Ville is located in.

In the Mekong River Delta study area, rice is grown almost exclusively (Truong et al., 2024). The only difference between fields is therefore the agricultural management, like when sowing, flooding, or harvesting is taking place. With multiple dates being examined, capturing various vegetative states, all fields in the study area can be
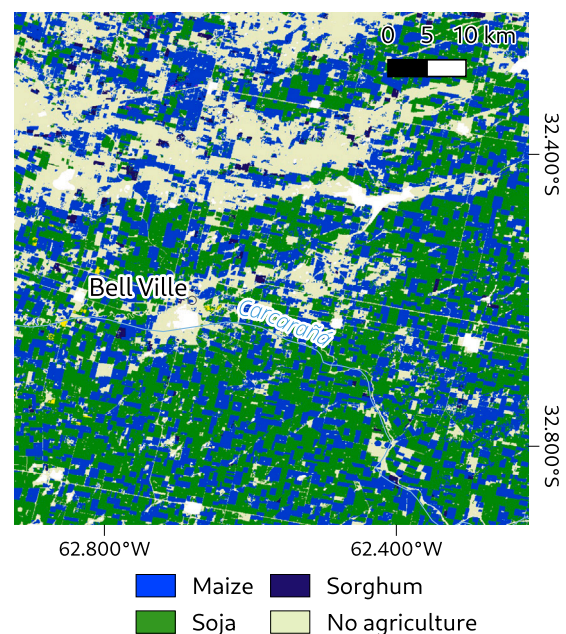
Fig. 3. Crop type map for the Bell Ville study area in Argentina for the winter season 2024. The classified crops are from the Argentina National Map of Crops (de Abelleyra et al., 2024).

considered to belong to the same class and should exhibit the same SAR–NDVI relationship.

In the Boort study region, crop classifications for the investigated years were unavailable. To still analyze the behavior of different crop types, one option is to apply unsupervised clustering to the fields. However, examining relationships among clusters with unknown properties and compositions yields very few insights. Therefore, no separate analysis per crop or cluster is carried out.

3. Methods

In the following sections, the perquisites for the data analysis are detailed. This includes SAR and optical data processing in Sections 3.1 and 3.2 and ends with a description of the data analysis methods (Section 3.3).

3.1. SAR data processing

The SAR data used in this study is sourced from different sensors and each sensor needs different processing steps to yield data suitable for analysis.

For the NovaSAR-1 data, both ScanSAR detected (SCD) and Analysis Ready Data (ARD) products were utilized. To the SCD data, we applied terrain correction and calibration in order to convert the digital numbers (DN) to $\sigma°$ intensity values. The ARD products that were utilized were already multi-looked, geocoded, and had undergone radiometric terrain flattening resulting in $\gamma°$ backscatter intensities. Accordingly, the ARD intensity data were solely transformed to a logarithmic scale. It should be noted that neither the SCD nor the ARD products include any corrections for antenna patterns or scalloping effects.

The processing of Sentinel-1 data was performed in a standard manner: precise orbit application, thermal and border noise removal, calibration, and geocoding. The processing chain for SAOCOM data included calibration to intensity values, multi-looking with 1×3 looks in range $\times$ azimuth, conversion from slant range to ground range, and geocoding. COSMO-SkyMed (CSG) data processing involved 3×3 multi-looking and geocoding. Sentinel-1, SAOCOM and CSG data are normalized to $\sigma°$ backscatter coefficients.

For processing the Sentinel toolbox SNAP was employed. Geocoding was performed using the Copernicus 30 m Digital Elevation Model (DEM). All data were converted to intensity values on a logarithmic scale, expressed in decibels (dB).

Given that all sensors provided both cross- and co-polarized data, the cross-ratio can be calculated by dividing the co-polarized data by the cross-polarized data, with both polarizations expressed in a linear scale: $\frac{\text{co-pol}}{\text{cross-pol}}$. If the values are expressed in a logarithmic scale, this results in a subtraction of the decibel values. The combination of both polarizations into a single value enables a joint analysis of both polarizations and may potentially enhance the strength of the relationship. As the sensors provide different polarizations, different cross-ratios can be calculated: $^{HH}/_{HV}$, $^{VV}/_{HV}$, or $^{VV}/_{VH}$.

Next to the cross-ratio, the radar vegetation index (RVI) is calculated. Originally, it was defined for quad-polarized data (Kim and van Zyl, 2000) combining three polarization:

$$\text{RVI} = \frac{8\sigma_{HV}}{\sigma_{HH} + \sigma_{VV} + 2\sigma_{HV}}. \tag{1}$$

However, often only two polarizations are acquired with one transmit and two receive polarizations. Therefore, the RVI is adapted assuming that the cross- and the two co-polarized data are identical, e.g. $\sigma_{HH} = \sigma_{VV}$ and $\sigma_{VH} = \sigma_{HV}$. Then, the RVI using only two polarizations can be calculated (Trudel et al., 2012; Nasirzadehdizaji et al., 2019):

$$\text{RVI}_{VV,VH} = \frac{4\sigma_{VH}}{\sigma_{VV} + \sigma_{VH}} \tag{2}$$

$$\text{RVI}_{HH,HV} = \frac{4\sigma_{HV}}{\sigma_{HH} + \sigma_{HV}}. \tag{3}$$

The geolocation accuracy of several SAOCOM and NovaSAR-1 scenes was insufficient, which required a manual correction. As this was done solely on the processed data, minor inaccuracies were introduced during the SAR processing due to the mislocated DEM and potentially erroneous incidence angles. However, these errors are sufficiently small to not affect the results. The geolocation accuracy of NovaSAR-1 is particularly poor when the satellite state vector is based on two-line element (TLE) data, as opposed to the more accurate GPS. The use of ground control points has the potential to enhance the SAR orthorectification, as demonstrated in Joshi et al. (2022), but was not used in this study due to the manual effort required for accurately acquiring them.

For one Sentinel-1 acquisition in Australia, implausibly low VH SAR backscatter values occur with median values of fields of −40 dB. This is the result of SNAP's thermal noise removal, where pixels with backscatter values below zero are clipped and set to 1×10^{-5} (or

−50 dB). After subsequent processing and resampling steps, this results in backscatter values dropping below −45 dB. To address this issue, any fields with more than 5% of pixels below −45dB are excluded for the analysis. Furthermore, in all remaining fields, pixels with values less than −45 dB are masked.

3.2. Optical data processing

Sentinel-2's optical data and the NDVI calculated from it are employed to establish a relationship with the SAR backscatter data. The optical data comes with a scene classification map (SCL), which contains information about the depicted object or surface of each pixel like clouds or snow. This mask is used to mask cirrus and other clouds as well as their shadows. Consequently, only those pixels classified as either *vegetated* or *non-vegetated* are kept. The SCL mask is upsampled from a resolution of 20 m to 10 m using nearest neighbor upsampling, as the used multi-spectral bands have a resolution of 10 m.

The NDVI is calculated using the red (R) and infrared (NIR) bands, specifically Sentinel-2 bands B04 and B08, using

$$\text{NDVI} = \frac{\text{NIR} - \text{R}}{\text{NIR} + \text{R}} \tag{4}$$

To ensure numerical stability and avoid divisions by zero, a small positive number can be added to the denominator.

In the Mekong River Delta, the rice paddy fields are flooded at the beginning of the season. As the classification of *water* in the SCL was insufficient in detecting this flooding, we additionally calculate the modified normalized difference water index (mNDWI) (Xu, 2006). The mNDWI utilizes green (G) and short wave infrared (SWIR) spectral bands, for which we chose Sentinel-2 bands B03 and B11, respectively, with the following equation

$$\text{mNDWI} = \frac{\text{G} - \text{SWIR}_1}{\text{G} + \text{SWIR}_1} \tag{5}$$

As Sentinel-2's SWIR channel B11 is acquired at a resolution of 20 m, we upsampled it to 10 m resolution using bilinear interpolation. During data analysis, the mNDWI value is used to filter out fields that are potentially flooded, as described in the following Section 3.3.

3.3. Data analysis

For this study, a field-wise approach was employed for data analysis to assess the relationship between SAR backscatter and NDVI values. A preliminary pixel-wise analysis did not show a significant relationship between them, which is likely due to the strong influence of speckle. This is also described in Roßberg and Schmitt (2024), where a pixel-wise analysis yielded inconclusive results.

The delineated field polygons were used to extract the median values from the SAR and optical raster images. Taking the median mitigates the impact of speckle and noise and enhances the reliability of the data. In the case of the Mekong River Delta study area, flooded fields with an average mNDWI above 0.2 were excluded to ensure that only relevant agricultural fields were analyzed.

To quantify the linear relationship between the SAR backscatter and NDVI values, Pearson's ρ correlation coefficient was employed. Pearson's ρ is a statistical measure that ranges from −1 to 1, indicating a perfect negative to perfect positive linear correlation, with 0 signifying no relationship. As Pearson's ρ is sensitive to outliers, extreme values were masked in the analysis. If a field has a mean NDVI or backscatter within the top or bottom 1% of all fields, it is excluded. The calculation of ρ was performed using the Python package SciPy.

Scatter plots were generated to visualize the relationship between backscatter and NDVI values. An ideal scenario would be a 1:1 mapping where each backscatter value directly corresponds to an NDVI value, which would imply a perfect linear relationship. This visualization aids in assessing the potential for direct translation of backscatter data to NDVI values, which is crucial for evaluating the suitability of SAR data, particularly at the S-band, for vegetation monitoring and NDVI estimation.

4. Results

The results of each study area are presented in the following subsections.

4.1. Bell Ville (Argentina)

The NDVI values for all fields fall between 0.2 and 1, indicating that the data encompass all vegetative stages, from barren to fully grown fields. Values around 0.25 and 0.9 are more common than values situated between these distribution peaks.

Both NovaSAR-1 and Sentinel-1 backscatter distributions are approximately bell-shaped but differ in magnitude. Co-polarized backscatter values exceed cross-polarized ones by 10 dB.

For both polarizations HH and HV of the NovaSAR-1 data a positive relationship with the NDVI is evident, whereby an increase in backscattered energy corresponds with an increase in NDVI values, which can be seen in Fig. 4. The relationship between cross-polarized HV data is higher than for cross-polarized HH data, which can be numerically verified by the high ρ of 0.68 and a weak ρ of 0.35, respectively, as listed in Table 5. Using the cross-ratio $^{HH}/_{HV}$ or the RVI results in a moderate relationship with ρ of -0.48 or 0.46, respectively.

These numeric results can be confirmed visually when analyzing the resulting scatter plots (see Fig. 4). While for the HV polarized backscatter the points follow a line more closely, they are more dispersed for HH data. For both cross-ratio and RVI, there is a clearly visible relationship, which is more dispersed than the HV data but not as much dispersed as the HH data. The local incidence angle, ranging from 23° to 31°, influences the backscatter values with higher backscatter occurring for lower incidence angles. Also RVI and cross-ratio are influenced by the local incidence angle.

The results for the Sentinel-1 data are similar to the NovaSAR-1 data only for the cross-polarized backscatter with a strong relationship being observed ($\rho = 0.68$). In contrast to the results with NovaSAR-1, also for Sentinel-1's co-polarized VV backscatter a strong relationship is found ($\rho = 0.62$), but no relationship with either RVI or cross-ratio $^{VV}/_{VH}$ is discernible. Another difference is between Sentinel-1 and NovaSAR-1 data is less variation of the local incidence angle, which ranges only between 35° and 36.5°. Visually, a clearly discernible relationship between backscatter of both polarizations is found as illustrated in Fig. 5

To analyze the SAR–NDVI-relationship separately for each crop, the Argentine National Map of Crops is utilized, which is shown in Fig. 3. Only two crops are dominant for the labeled fields with 40% of the fields having soybean grown on them ($N = 83$) and 37% maize ($N = 75$). The remainder of the fields are categorized as "no cropland" ($N = 46$), which includes grasslands and pastures.

For Soybean, both Sentinel-1 polarizations achieve a very strong relationship with the NDVI values ($\rho > 0.8$), whereas with NovaSAR-1 data, only the cross-polarized HV backscatter is strongly related ($\rho = 0.74$). NovaSAR-1 HH data is weakly related to the NDVI for soy beans ($\rho = 0.32$). The magnitude of ρ is very similar for the RVI and cross-ratios for all crops, as listed in Table 5. Despite the better relationship of the Sentinel-1 backscatter with NDVI values compared to NovaSAR-1, the RVI and $^{HH}/_{HV}$ cross-ratio calculated using NovaSAR-1 data is better related to the NDVI ($|r|$ 0.45 for NovaSAR-1, $|r| \approx 0.3$ for Sentinel-1).

For maize, NovaSAR-1 backscatter values related similar strongly with NDVI data as for soybean ($\rho = 0.69$ and 0.34 for HV and HH data), which is depicted in Fig. 6. In contrast, Sentinel-1 backscatter values are related less strongly with NDVI values for Maize fields than for Soybean fields as shown in Fig. 7. However, the there is still a moderate to strong positive relationship found ($\rho = 0.62$ and 0.54 for VH and VV backscatter). The magnitude of ρ for cross-ratio and RVI of both sensors is similar between soybean and maize fields. Notably, in the case of Sentinel-1's cross-ratio $^{VV}/_{VH}$ and RVI, the sign of the relationship changes. Visually, for both soybean and maize fields, no

proper relationship between NDVI data and either RVI or cross-ratio of Sentinel-1 data can be confirmed, which is illustrated for the RVI in Fig. 7(c).

For grasslands and pastures ("no cropland"), the relationship between NDVI and SAR data is weak across sensors, polarizations and ratios. The best relation is found for Sentinel-1's RVI with a correlation coefficient ρ of -0.36. Despite this weak relationship, visually no such relationship is discernible as shown in Fig. 7(c).

The Pearson's correlation coefficient ρ for both NovaSAR-1 and Sentinel-1 data as given in Table 5. In that table, they are given for all fields together and also separately per crop type.

4.2. Boort (Australia)

In general, the findings for this study area are comparable to those of Boort, Australia, as previously presented in Section 4.1

A positive relationship between backscatter values and NDVI is evident for NovaSAR-1 cross-polarized HV data as shown in Fig. 8(b). No discernible relationship is evident between the backscatter values and the NDVI for both co-polarized waves HH and VV. This can be numerically verified by the moderately high ρ of 0.54 for HV, but the negligible low ones of 0.0 and -0.14 for HH and VV, respectively. Using the cross-ratio instead of single polarization does increase the relationship with NDVI values mildly for the $^{VV}/_{HV}$ cross-ratio to $\rho = -0.64$, but is in the same range for the $^{HH}/_{HV}$ cross-ratio with $\rho = -0.55$. The relationship strength between RVI and NDVI is in between the two cross-ratios and moderately strong with $\rho = 0.59$. Visually, a better relationship with NDVI values of the cross-ratio data compared to the HV polarization cannot be clearly attested. The local incidence angle influences the backscatter values with higher backscatter occurring for lower incidence angles. This effect does not occur for the cross-ratio. The scatter plots for all three NovaSAR-1 polarizations relating them to Sentinel-2 NDVI are presented in Fig. 8.

The results for the Sentinel-1 backscatter data are analogous to those observed for the NovaSAR-1 backscatter. Cross-polarized VH backscatter demonstrates a positive correlation with NDVI values, while no discernible relationship is evident in the case of co-polarized VV data. Once more, this yields a moderately high ρ value of 0.52 for VH polarization, but a ρ of zero for VV-polarization data.

As with the NovaSAR-1 data, the cross-ratio results in an improvement in the correlation coefficient, ρ, for Sentinel-1 data, with a value of 0.52 for VH polarization and -0.74 for the cross-ratio $^{VV}/_{VH}$. While this effect is not readily apparent in visual inspection, it may be present, as evidenced by the scatter plots in Fig. 9 that compare NDVI data with VH and VV polarizations and the cross-ratio. The RVI achieves the highest relationship with the NDVI with $\rho = 0.82$.

The correlation coefficient ρ for the two sensors, their polarizations, and cross-ratio is given in Table 6.

4.3. Mekong River Delta (Vietnam)

The results of the Mekong River Delta study area differ from those of the previous two regions. The results demonstrate that, in the case of NovaSAR-1 S-band data, the HH polarized data exhibits a positive correlation with NDVI values, rather than the HV polarized data, which is shown in the scatter plots in Fig. 10. This can be confirmed by the high correlation coefficient for HH data with $\rho = 0.51$ compared to $\rho = 0.15$ for HV data. Additionally, only the cross-ratio $^{HH}/_{HV}$ is achieving a moderate relationship with the NDVI with $\rho = 0.51$, while no relationship is found for the RVI. As observed in the previous two study regions, the incidence angle influences the backscatter values.

A similar pattern to NovaSAR-1 data is observable for Sentinel-1 data: co-polarized VV data exhibits a high negative relationship with NDVI values with $\rho = -0.59$ but cross-polarized data shows no relationship with the NDVI with $\rho = -0.02$. The cross-ratio $^{VV}/_{VH}$ and the RVI exhibits a similar relationship with the NDVI as the HV polarized

(a) HV backscatter

(b) HV backscatter

(c) RVI
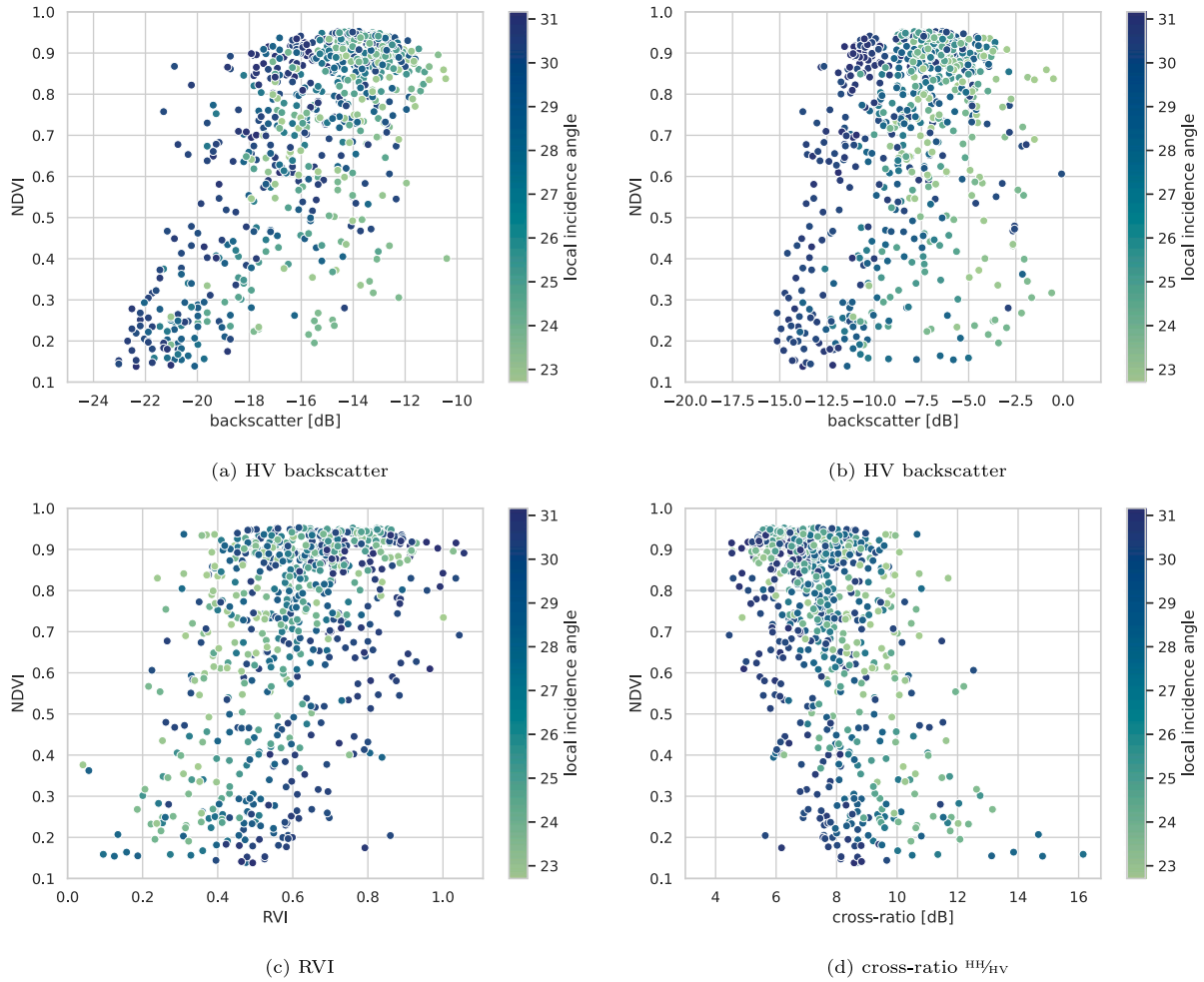
(d) cross-ratio $^{HH}/_{HV}$

Fig. 4. Comparison of NDVI and NovaSAR-1 data for the HH and HV polarized backscatter as well as the RVI and the cross-ratio $^{HH}/_{HV}$ for the Bell Ville study area in Argentina. The local incidence angle is indicated for each data point by its color. (For interpretation of the references to color in this figure legend, the reader is referred to the web version of this article.)

(a) VH backscatter

(b) VV backscatter
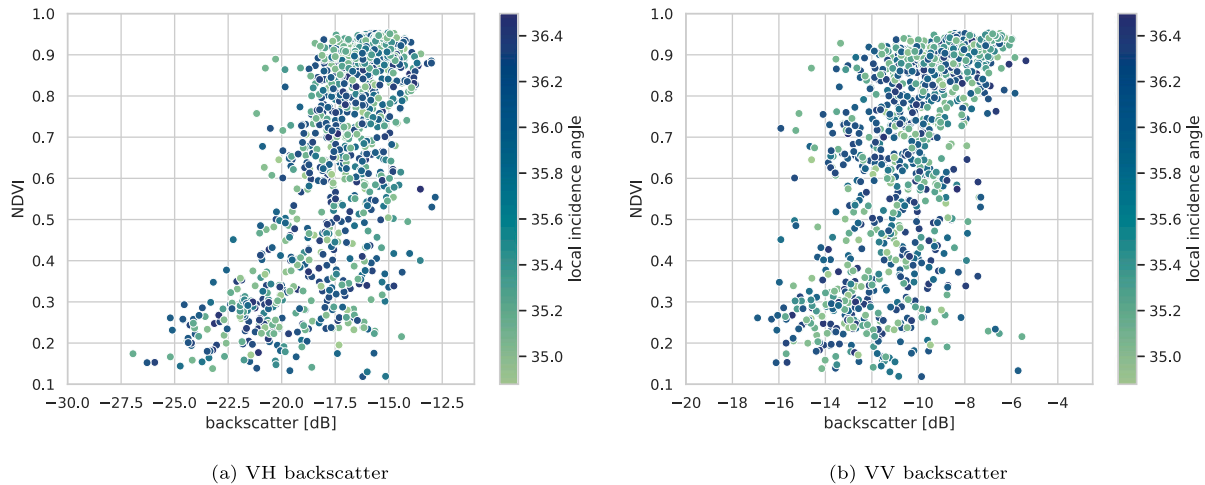
Fig. 5. Comparison of NDVI and Sentinel-1 data for the two polarizations VV and VH for the Bell Ville study area in Argentina. The local incidence angle is indicated for each data point by its color.
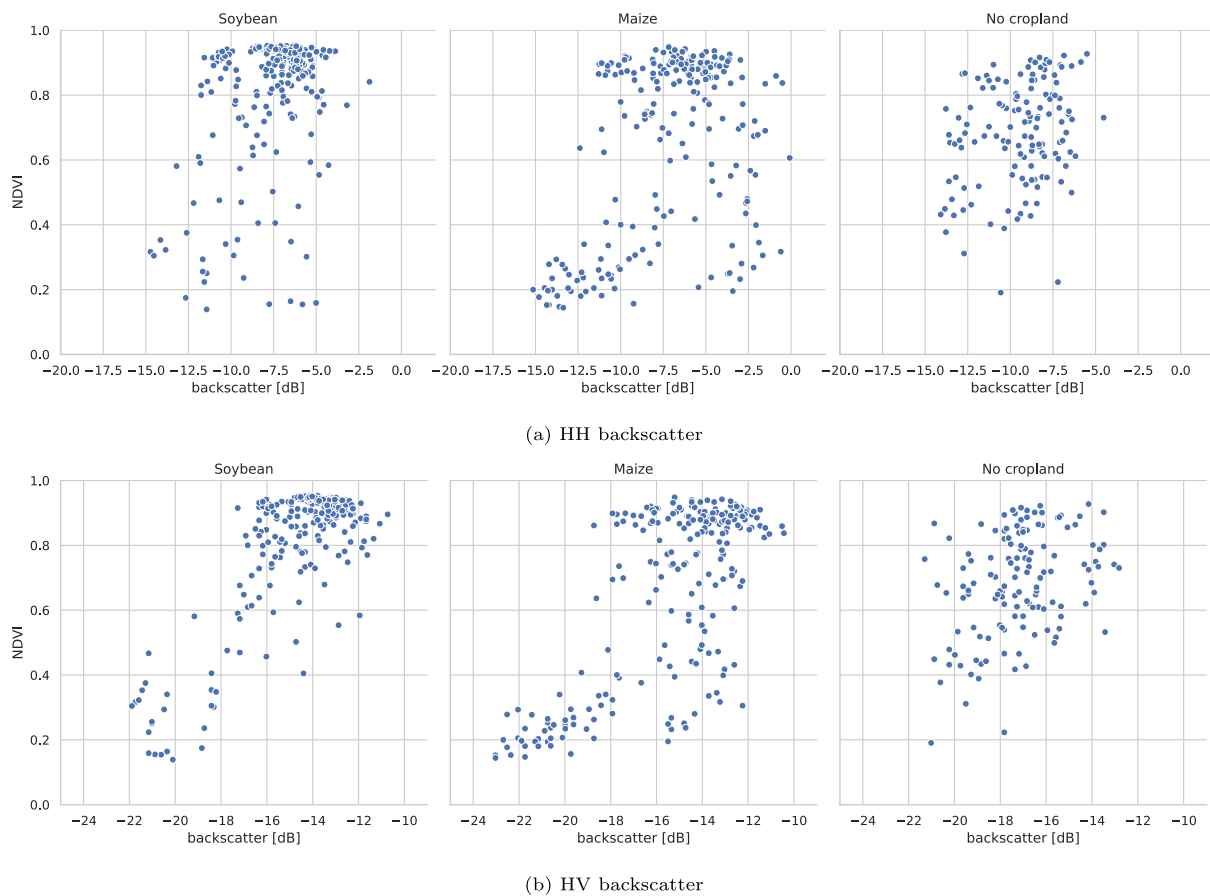
(a) HH backscatter

(b) HV backscatter

Fig. 6. Relationship between NovaSAR-1 SAR backscatter and NDVI data for the Bell Ville study area in Argentina given for each of the three classified crops.

Table 5
Relationship between NDVI values and SAR data for the study area Bell Ville (Argentina). Next to the polarizations, the cross-ratios and RVI are displayed. ρ denotes the Pearson's correlation coefficient and N the number of samples.

Sensor	Data	All fields		Soybean		Maize		No cropland	
		ρ	N	ρ	N	ρ	N	ρ	N
NovaSAR-1	HV	0.68	(706)	0.74	(238)	0.69	(214)	0.33	(128)
	HH	0.35	(703)	0.32	(238)	0.34	(212)	0.25	(128)
	$^{HH}/_{HV}$	−0.48	(704)	−0.49	(239)	−0.50	(212)	0.04	(129)
	RVI	0.46	(704)	0.46	(239)	0.50	(212)	−0.03	(129)
Sentinel-1	VH	0.68	(1096)	0.80	(387)	0.62	(340)	0.34	(193)
	VV	0.62	(1095)	0.89	(387)	0.54	(340)	0.28	(192)
	$^{VV}/_{VH}$	−0.10	(1097)	0.30	(390)	−0.37	(340)	−0.36	(194)
	RVI	0.05	(1095)	−0.34	(388)	0.34	(339)	0.27	(193)

data with $\rho = -0.62$ and $\rho = 0.61$, respectively. When analyzing the scatter plots in Fig. 11, the distribution for VH data exhibits two regions. The first region encompasses higher NDVI values above 0.25, where a negative relationship appears to be present. In contrast, a positive relationship is observed for the second region encompassing NDVI values below 0.25. This can be verified by calculating ρ separately for fields with NDVI values above and below 0.25. For vegetated fields (NDVI> 0.25) a moderate negative relationship is found with $\rho = -0.43$, whereas for fields with NDVI< 0.25 a weak positive relationship is found with $\rho = 0.32$. The relationship between backscatter and NDVI is illustrated in Fig. 11.

For COSMO-SkyMed (CSG) X-band data, the cross-polarized HV data seems to have a negative relationship with the NDVI data with $\rho = -0.59$. In contrast, the co-polarized HH data exhibits no discernible relationship. Both RVI and cross-ratio $^{HH}/_{HV}$ achieve a moderately strong relationship with the NDVI of $\rho \approx 0.6$. As CSG data were only available for a single date in August the amount of samples and data

diversity is limited which decreases the certainty of the results. Scatter plots of both polarizations are given in Fig. 12.

The L-band SAOCOM data represents the fourth investigated SAR frequency and appears to have no discernible relationship with the NDVI data. All backscatter values in both HV and HH polarizations occur for all NDVI values. This is shown in Fig. 13 and confirmed by correlation coefficients ρ of 0.0 and −0.18 for HH and HV polarization, respectively. Only the cross-ratio $^{HH}/_{HV}$ and the RVI exhibits a slightly higher $|\rho|$ of 0.24, indicating a very weak relationship.

An overview of all Pearson's correlation coefficients of the different sensors, their polarizations, and cross-ratios is given in Table 7.

5. Discussion

This study investigates the relationship between the SAR backscatter of different frequencies and the NDVI. The findings suggest a relationship between NDVI and C- and S-band SAR backscatter and potentially
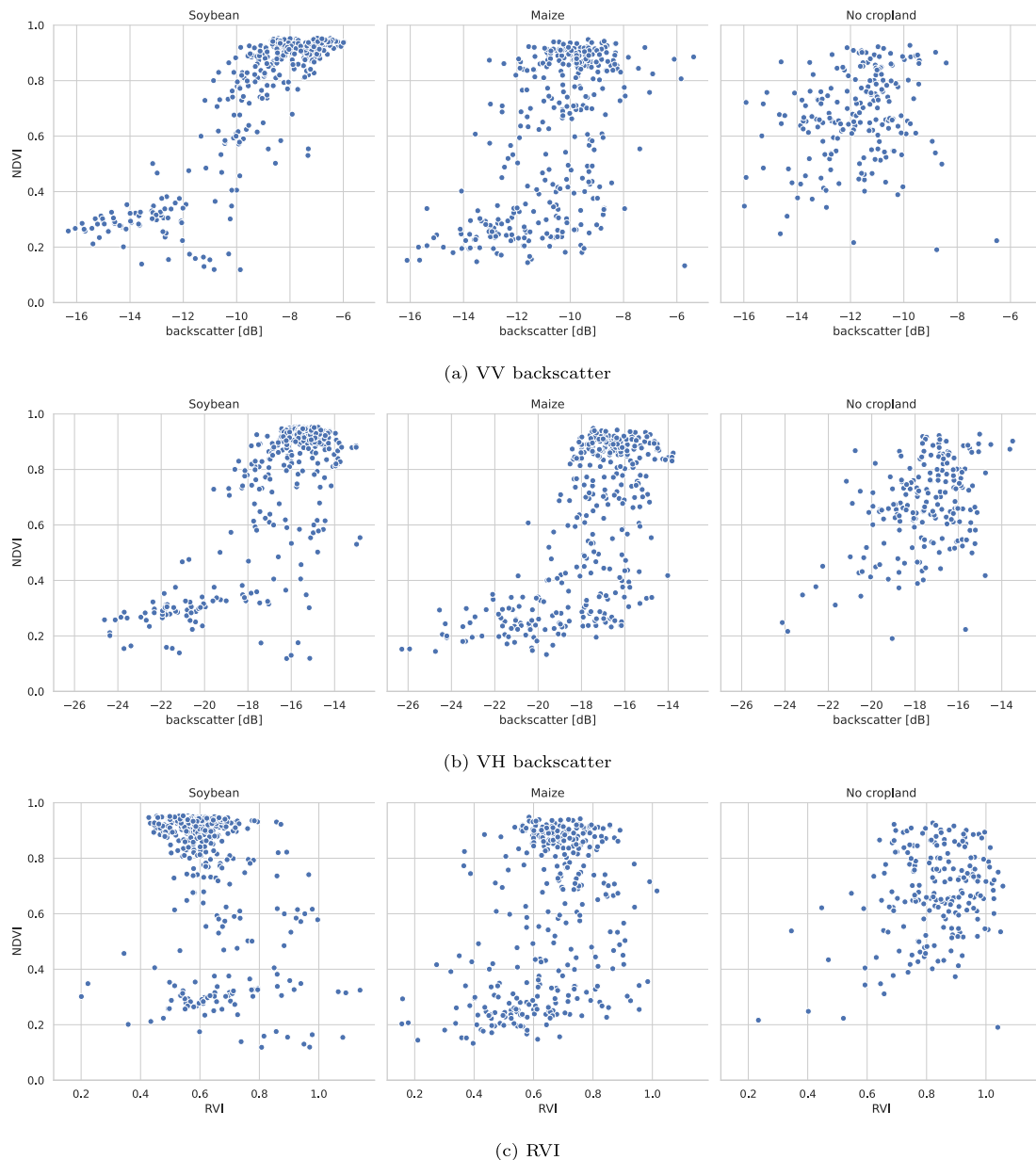
(a) VV backscatter

(b) VH backscatter

(c) RVI

Fig. 7. Relationship between Sentinel-1 SAR data and NDVI data for the Bell Ville study area in Argentina given for each of the three classified crops.

Table 6

Relationship between NDVI values and SAR data for the study area Boort (Australia). Next to the polarization, the cross-ratio and the RVI formed from them is used. ρ denotes the Pearson's correlation coefficient and N the number of samples.

Sensor	Data	ρ	N
NovaSAR-1	HV	0.54	(366)
	HH	0.00	(366)
	VV	−0.14	(366)
	$^{HH}/_{HV}$	−0.55	(366)
	$^{VV}/_{HV}$	−0.64	(366)
	RVI	0.59	(366)
Sentinel-1	VV	0.00	(455)
	VH	0.52	(455)
	$^{VV}/_{VH}$	−0.74	(457)
	RVI	0.82	(457)

The analysis encompassed three study areas with different characteristics. The results for two areas, Boort (Australia) and Bell Ville (Argentina), indicate a strong correlation between S- and C-band cross-polarized backscatter and NDVI. This is to be expected, as the volumetric scattering of vegetation increases with increasing vegetation volume, which in turn leads to higher cross-polarized responses (Flores et al., 2019). In Bell Ville, not only cross-polarized but also co-polarized S- and C-band data exhibited a notable relationship with the NDVI, which may be due to the different crop types. While broad-leaf crops like soybeans and maize are the predominant crops in Bell Ville, narrow-leaf crops like wheat and barley are the primary crops in Boort (cf. Section 2.1). The distinct backscatter characteristics of these two crop types (Macelloni et al., 2001) may be responsible for the different backscatter–NDVI relationships observed. For instance, one study demonstrated that the crop height of corn, a broad-leaf crop, exhibits a good relationship with both HH and HV C-band RADARSAT-2 backscatter. However, for wheat, a narrow-leaf crop, only HV polarized data demonstrated a significant relationship (Liao et al., 2017).
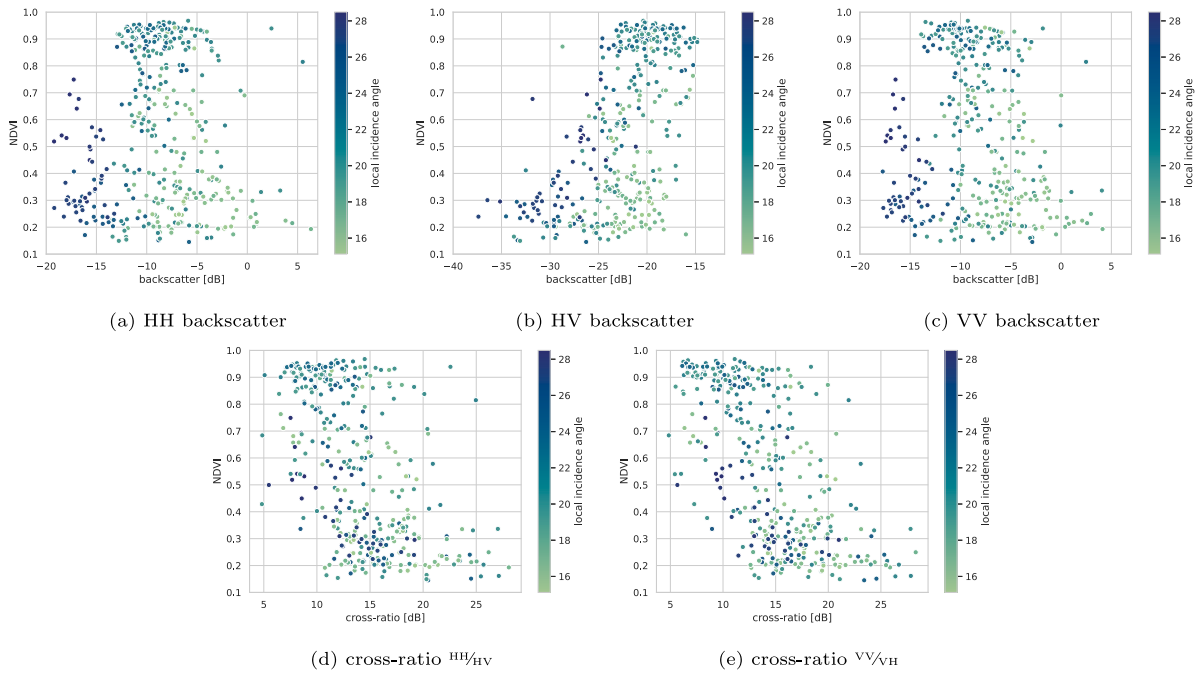
also with X-band data. However, no such relationship was observed in the L-band data.

Fig. 8. Comparison of NDVI and NovaSAR-1 data for the Boort study area in Australia. All three polarizations HH, HV, VV, and the two cross-ratios $^{VV}/_{HV}$ and $^{HH}/_{HV}$ which can be calculated from these polarizations are given. The local incidence angle of the SAR data is indicated by different colors. (For interpretation of the references to color in this figure legend, the reader is referred to the web version of this article.)
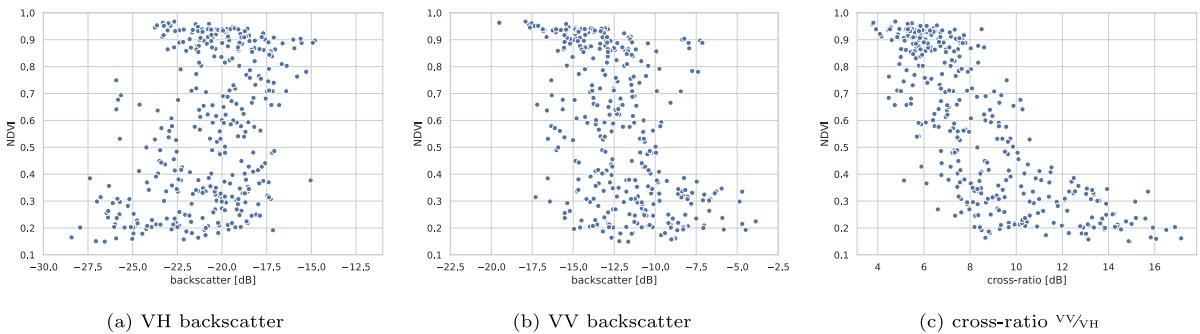

Fig. 9. Comparison of NDVI and Sentinel-1 data for the two polarizations VV, VH, as well as the cross-ratio for the Boort study area in Australia.
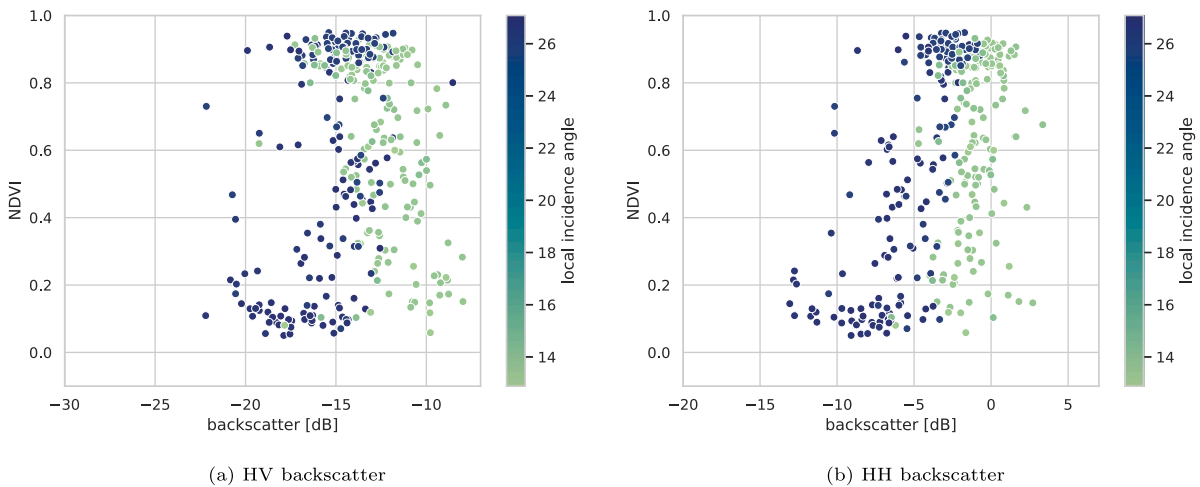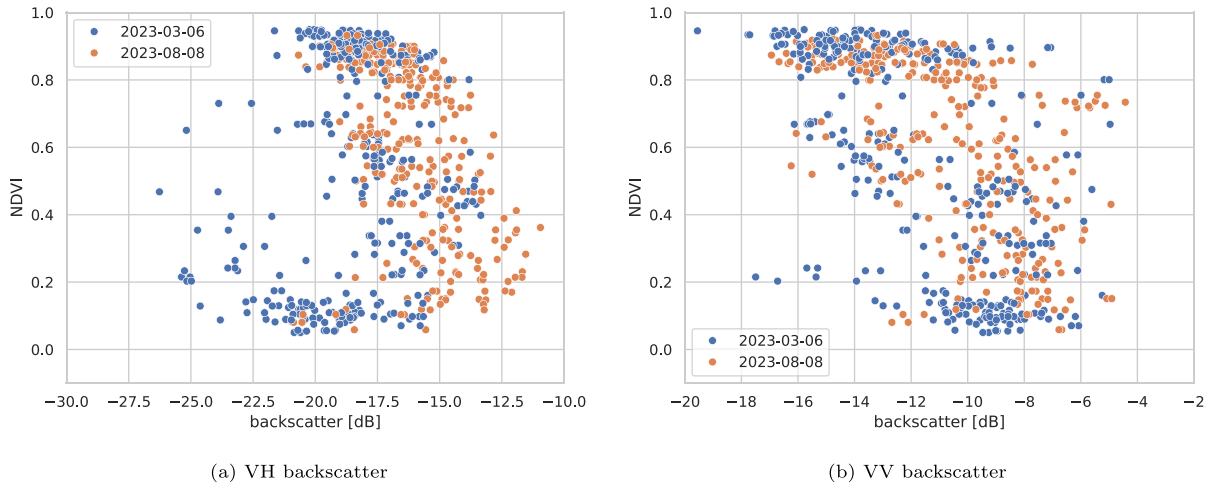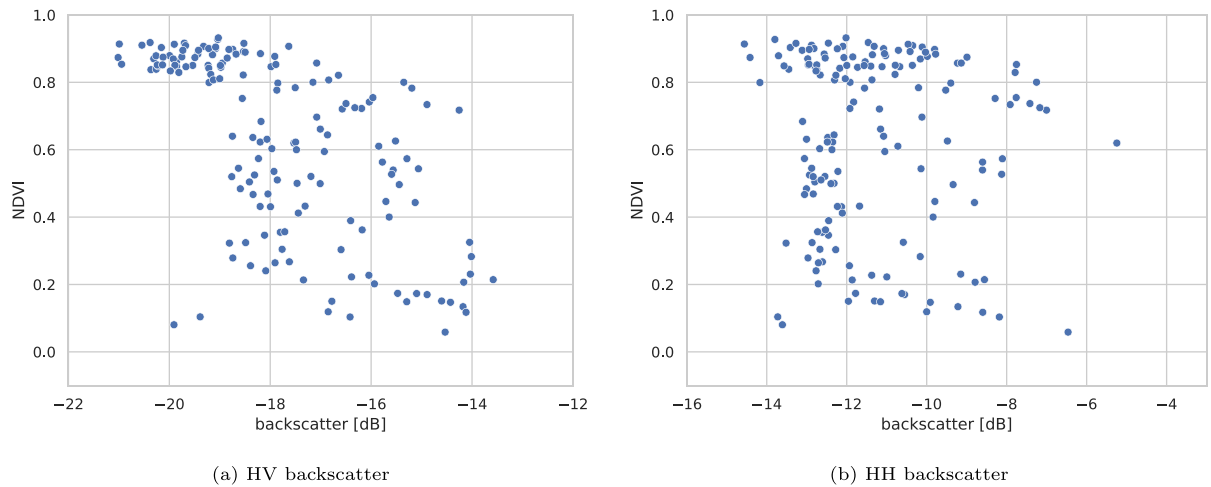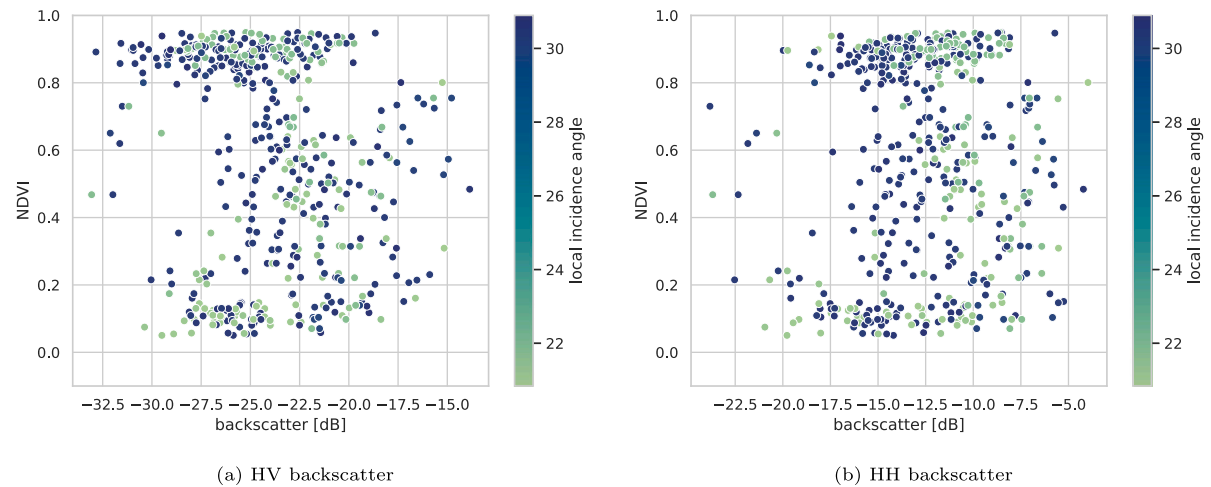

Fig. 10. Relationship between NovaSAR-1 backscatter and NDVI values for the Mekong River Delta study area in Vietnam. The local incidence angle of the NovaSAR-1 data is indicated for each data point by its color. (For interpretation of the references to color in this figure legend, the reader is referred to the web version of this article.)

(a) VH backscatter

(b) VV backscatter

Fig. 11. Relationship between Sentinel-1 backscatter and NDVI values for the Mekong River Delta study area in Vietnam. The Sentinel-1 acquisition data of each sample is indicated by its color. (For interpretation of the references to color in this figure legend, the reader is referred to the web version of this article.)

(a) HV backscatter

(b) HH backscatter

Fig. 12. Relationship between COSMO-SkyMed Second Generation (CSG) SAR backscatter and NDVI values for the Mekong River Delta study area in Vietnam.

(a) HV backscatter

(b) HH backscatter

Fig. 13. Relationship between SAOCOM SAR backscatter and Sentinel-2 NDVI values for the Mekong River Delta study area in Vietnam. The local incidence angle of the SAOCOM data is indicated for each data point by its color. (For interpretation of the references to color in this figure legend, the reader is referred to the web version of this article.)

Table 7

Relationship between NDVI values and SAR data for the study area Mekong River Delta (Vietnam). ρ denotes the Pearson's correlation coefficient and N the number of samples. Next to the polarization, the cross-ratio and the RVI formed from them is used. Additionally, for Sentinel-1 cross-polarized VH data, the relationship is given for NDVI values above and below 0.25, because two distinct relationships are apparent in the scatter plot of the data (cf. Fig. 11).

Sensor	Data	ρ	N
NovaSAR-1	HV	0.15	(313)
	HH	0.51	(313)
	HH/HV	0.51	(313)
	RVI	0.01	(313)
Sentinel-1	VV	−0.59	(633)
	VH	−0.02	(632)
	VV/VH	−0.62	(629)
	RVI	0.61	(629)
	VH for NDVI < 0.25	0.32	(143)
	VH for NDVI > 0.25	−0.46	(485)
CSG	HH	−0.01	(153)
	HV	−0.59	(152)
	HH/HV	0.61	(152)
	RVI	−0.63	(152)
SAOCOM	HH	0.00	(478)
	HV	−0.18	(478)
	HH/HV	0.24	(479)
	RVI	−0.24	(479)

The results for Sentinel-1 C-band data are in line with the existing literature. Villarroya-Carpio and Lopez-Sanchez (2023) could show, that there exists a good relationship between the NDVI and both cross-ratio and RVI of Sentinel-1 data next to the coherence. The strength of the relationship is very different for the crops of the investigated fields located in Spain. While for instance a very strong relationship is found for Maize or Rice ($R^2 > 0.6$ for a linear fit for all of the five investigated years), the relationship is less strong and more variable for Wheat (R between 0.4 and 0.75). For chickpeas, which belong to the Leguminosae subfamily like soy beans and have a similar plant structure, the relationship is strong for all but one year with R^2 above 0.5.

Holtgrave et al. (2020) investigate the relationship between NDVI and Sentinel-1 SAR data for agricultural fields and grasslands in Northern Germany and also find a good relationship between both. They find the strongest relationship for Maize, with the single VH polarization being better than the cross-ratio or RVI and the VV polarized data having the weakest relationship. This is similar to the results we report for Maize in the Bell Ville study area in Table 5, where we find VV polarized data to having the best relationship. For grasslands, the results are also similar, with a generally weaker relationship (ρ around 0.3). The only difference is, that we still find a relationship between VV polarized backscatter values with the NDVI for grasslands ($\rho = 0.28$), while Holtgrave et al. (2020) do not find this ($\rho = 0.11$).

A third study investigating C-band data also finds a relationship between backscatter and NDVI values for winter wheat fields in India, with a negative ρ for the cross-ratio VV/VH (Pandit et al., 2023).

Contrastingly, the third study area comprising rice paddy fields in Vietnam exhibited distinctive backscatter characteristics that set them apart from the other two regions. For these fields, co-polarized HH and VV data were related to NDVI, while cross-polarized HV and VH data were not. It is unclear, why a relationship can be found only for co-polarized and not cross-polarized data, especially given that other researchers have identified a relationship between plant parameters and backscatter for paddy rice. For instance, the cross-polarized backscatter of a ground-based scatterometer has been demonstrated to relate well to the leaf area index (LAI), fresh weight or biomass, and canopy height (Inoue et al., 2002; Jia et al., 2014). Additionally,

RADARSAT-2 backscatter and phenology are linked for rice (Lopez-Sanchez et al., 2014). Another particularity of the cross-polarized VH C-band data is the existence of two distinct relationships between C-band VH backscatter and NDVI values, one for NDVI values below and another one for values above 0.25. A possible explanation for this phenomenon is that low NDVI values, which are likely due to the presence of water surfaces without much vegetation cover, result in a low backscatter, which is to be expected given that water acts as a specular surface and mirror, reflecting most of the signal's energy away from the sensor. As more of the surface is covered by rice and not by water, the NDVI as well as the backscatter increase because the surface becomes less specular. As the NDVI increases above 0.25, a negative relationship between NDVI and VH backscatter occurs with a VH backscatter decrease for increasing NDVI values. The reason for this behavior is currently unknown. It is similarly unclear, why these two relationships could not be observed for S-band data. One potential explanation might be attenuation whereby the vertically polarized waves interact strongly with the vertically oriented rice stalks leading to some attenuation. It remains unclear, why volumetric scattering which leads to a high cross-polarized response and is typically high for dense vegetation, is not the dominant factor in this case.

An unknown factor influencing the result might be the availability of optical imagery. In the event that optical data is only available for certain vegetative periods, a comprehensive analysis cannot be conducted. In particular, if the monsoon period, which is often accompanied by heavy cloud cover, coincides with the transplanting of rice and the early growth stages, when the NDVI increases, then no data may be suitable for analysis. For rice, this presents a more significant challenge, as the crop develops from seedlings to mature plants in less than 30 days, and the NDVI increases from approximately zero to nearly one during this period (Onojeghuo et al., 2018). Capturing this rapid change is difficult due to the frequent cloud cover. Consequently, only the later vegetative stages can be readily captured with optical data and analyzed.

The different signs of ρ of S-band HH and C-band VV backscatter indicating positive and negative relationships can be explained by the geometric properties of the rice plants. One strong scattering effect for this area with the inundated surface is double bounce, which typically results in a higher HH response (Flores et al., 2019). Additionally, the vertical orientation of the rice stems contributes to the higher HH response relative to the VV one (Oh et al., 2009).

5.1. L- and X-band sensitivity to vegetation indices

No discernible relationship was observed between L-band backscatter and NDVI values. This finding is surprising, as other studies have demonstrated that L-band backscatter is highly sensitive to the leaf area index (LAI) of rice (Inoue et al., 2002; Kim et al., 2013), and a relationship exists between LAI and NDVI (Zhou et al., 2017). However, no clear explanation for the lack of a relationship could be identified. While saturation of the NDVI at high biomass and LAI values may explain the disconnect at late vegetation stages, and the double-bounce effect could be influencing early growth stages, these factors should similarly affect relationships at other SAR frequencies. A possible explanation is provided by Paloscia (2002), who observed differences in biomass sensitivity between broad-leaf and narrow-leaf crops, such as rice. Specifically, L-band data proved more effective for broad-leaf crops, while C-band data showed greater suitability for narrow-leaf crops. This aligns with findings by Hosseini and McNairn (2017), who noted that RADARSAT C-band data outperformed UAVSAR L-band data in estimating wheat biomass, a crop with a similar plant structure to rice.

The results for the X-band data were inconclusive due to the availability of only one suitable scene. A relationship between cross-polarized HV data and NDVI may exist, but this is not the case for HH co-polarized data. This finding is inconsistent with the results of other

research, which demonstrated a relationship between HH X-band data and NDVI values as well as leaf area index (LAI) for 30 flooded rice paddy fields with a high ρ of 0.584 (Hirooka et al., 2015).

However, another study investigated wheat and barley, which have a similar plant structure to rice but are not cultivated on flooded fields, and demonstrated a negative relationship between co-polarized HH and VV X-band data and LAI (Fontanelli et al., 2013). Consequently, further research is required to examine the behavior of X-band data in relation to the NDVI and plant parameters.

5.2. Effectiveness of the cross-ratio and RVI

This study also evaluated the effectiveness of the cross-ratio (CR), finding it beneficial only in certain cases, dependent on the specific study area and sensor used. In a few areas, the relationship between CR and NDVI values was comparable or slightly stronger than that observed with a single polarization. If a study would like to use only one feature, calculating the CR would make selecting the optimal polarization unnecessary. However, in some cases, no relationship between CR and NDVI could be demonstrated, whereas with a single polarization a relationship existed. This illustrates, that no universal guidance can be derived from the data, and in each case, the utility of the CR must be reassessed.

For the radar vegetation index (RVI), results mirrored those observed with the cross-ratio. In some instances, the RVI showed a stronger relationship with the NDVI than single polarizations; however, more often, the relationship was weaker or even nonexistent.

5.3. Exploring the relationship between NDVI and interferometric coherence

Although interferometric coherence is a valuable indicator of vegetation state, particularly for short temporal baselines (Villarroya-Carpio and Lopez-Sanchez, 2024), it was not analyzed here. This is primarily due to limitations in data availability. Of the four investigated SAR sensors, only the full Cosmo-SkyMed constellation, comprising both first and second-generation satellites, can provide interferometric acquisitions with a temporal baseline between one to six days. This could warrant a separate investigation, but similar X-band data of the TerraSAR-X, TanDEM-X, and PAZ sensors has already been investigated (Villarroya-Carpio and Lopez-Sanchez, 2024). There it could be shown, that the NDVI is highly correlated with the coherence for short temporal baselines.

The Sentinel-1 mission allows interferometric analysis, but currently only for a temporal baseline of 12 days due to the failure of Sentinel-1B at the end of 2021. Such a long temporal baseline is unsuitable for most vegetation types. Following the launch of Sentinel-1C at the end of 2024 and completing its commissioning phase, temporal baselines of six days will once again be available for this C-band sensor.

NovaSAR-1 and SAOCOM are unsuitable for interferometric analysis of vegetation. Their orbital tubes are not narrowly controlled to maintain consistent spatial baselines. Only by chance a suitable spatial baseline for InSAR analysis is achieved (Li et al., 2022; Roa et al., 2021). This results in very long temporal baselines, significantly reducing the coherence for vegetated surfaces, rendering their data unsuitable for such an investigation.

In conclusion, although interferometric coherence holds promise for understanding vegetation states, its effective analysis is currently limited by the lack of suitable data. The main challenge is the necessity for frequent revisits to achieve adequately short temporal baselines.

5.4. Implications for SAR-based NDVI estimation

All these results show that the relationship between SAR backscatter and NDVI values is multifaceted and influenced by various factors. Our findings suggest that while a discernible relationship exists between backscatter and NDVI, its complexity is heightened by a number of factors. These include vegetation-related factors such as crop type, plant phenology, plant shape, or leaf arrangement; factors related to the SAR data such as SAR frequency and polarization; and geometric considerations including incidence angle and field orientation. In particular, different crop types, characterized by unique phenological stages, plant shapes, and leaf arrangements, exhibit varying backscatter responses. These findings underscore the challenges in developing a universal model for NDVI retrieval from SAR data due to the complex interplay of these factors. A generalized model would require the simultaneous disentanglement of the influence of all the different factors, which is a challenging task.

In conclusion, while this study confirms the relationship between SAR backscatter and NDVI for specific frequency bands and conditions, it also highlights several challenges and gaps that require further investigation to optimize SAR-based vegetation monitoring.

6. Conclusion

This paper examines the relationship between SAR backscatter data from multiple frequencies and the optically-derived normalized difference vegetation index (NDVI) in agricultural areas. The present study demonstrates that both C- and S-band cross-polarized backscatter (HV, VH) are associated with NDVI values, with the association also evident in some areas for co-polarized backscatter (HH, VV). Establishing this relationship is a prerequisite for reliably estimating NDVI values using SAR imagery, which combines both ease of use and application of vegetation indices with the all-weather imaging capabilities of SAR systems.

Three study areas with distinct climates and crops were selected for analysis, which are located in Argentina, Australia, and Vietnam. For these areas, data were acquired from the Sentinel-2 optical sensor, as well as from the NovaSAR-1 S-band, the Sentinel-1 C-band SAR sensor, and, in the case of Vietnam, the COSMO-SkyMed X-band and SAOCOM L-band SAR sensors. The NDVI showed a robust relationship with cross-polarized S- and C-band backscatter in the study regions of Australia and Argentina, with a Pearson correlation coefficient ρ exceeding 0.5. In the case of the Argentinean study area, the co-polarized backscatter also demonstrated a relationship with the NDVI, with correlation coefficients of $\rho = 0.35$ and $\rho = 0.62$ for the S- and C-band data, respectively. In Argentina, where crop type maps were available, a stronger relationship was observed for soybeans and maize, whereas meadows and grasslands showed a considerably weaker relationship. The results for the third study area in Vietnam, which is almost exclusively cultivated with rice, are in contrast to those of the other two areas. In this case, co-polarized S- and C-band backscatter relate to NDVI values with a correlation coefficient $\rho = 0.51$ and $\rho = -0.59$, respectively. For the same study area, X-band cross-polarized backscatter relates with NDVI ($\rho = -0.59$), yet no relationship could be shown for L-band data. The discrepancy in the strength of the relationship can be attributed to various factors, including the specific crop type and its structural characteristics, the utilized wavelength, and consequently, the SAR penetration depth.

In addition to single polarizations, the cross-ratio and the radar vegetation index (RVI) were included in the analysis. However, neither the cross-ratio nor the RVI consistently showed a stronger relationship with the NDVI than single polarizations, and in some cases, they showed no relationship at all.

The results indicate that NDVI can be linked to SAR backscatter across a range of frequencies. However, the results also show that no universal relationship exists; rather, various factors, including crop

type, agricultural practices, and SAR frequencies, influence the relationship between NDVI and SAR backscatter. In order to estimate NDVI values from the SAR backscatter, it might be necessary to provide the models with additional data beyond just the SAR backscatter, such as the crop type, or include SAR data of multiple acquisitions. Alternatively, complex models can be used to extract this information implicitly from the provided data. Following the launch of NISAR, its S- and L-band SAR sensors will provide a substantial amount of novel and supplementary data to Sentinel-1 C-band data. This will likely facilitate the development of models that use data from both sensors for precise NDVI retrieval on a global scale.

CRediT authorship contribution statement

Thomas Roßberg: Writing – review & editing, Writing – original draft, Visualization, Methodology, Investigation, Data curation, Conceptualization. **Michael Schmitt:** Writing – review & editing, Project administration, Funding acquisition, Conceptualization.

Declaration of competing interest

The authors declare that they have no known competing financial interests or personal relationships that could have appeared to influence the work reported in this paper.

Acknowledgments

Data availability

The code used for analysis, delineated field polygons and values extracted from the imagery are available at the Open DataHub of the University of the Bundeswehr (Roßberg and Schmitt, 2025) and additionally at https://github.com/oceanites/multifrequency-sar-ndvi-relationship.

References

U.S. Department of Agriculture, I.P.A.D.., 2024. Crop Calendars for Southern South America. URL https://ipad.fas.usda.gov/rssiws/al/crop_calendar/ssa.aspx.

Alvarez-Mozos, J., Villanueva, J., Arias, M., Gonzalez-Audicana, M., 2021. Correlation between NDVI and Sentinel-1 derived features for maize. In: Proceedings of IEEE International Geoscience and Remote Sensing Symposium. pp. 6773–6776. http://dx.doi.org/10.1109/igarss47720.2021.9554099.

Australian Bureau of Statistics, 2024. Australian agriculture: Broadacre crops. URL https://www.abs.gov.au/statistics/industry/agriculture/australian-agriculture-broadacre-crops/2022-23.

Baup, F., Villa, L., Fieuzal, R., Ameline, M., 2016. Sensitivity of X-Band (σ^0, γ) and optical (NDVI) satellite data to corn biophysical parameters. Adv. Remote. Sens. 5 (2), 103–117. http://dx.doi.org/10.4236/ars.2016.52009.

Chuvieco, E., 2020. Fundamentals of Satellite Remote Sensing, Third Ed. CRC Press, Taylor & Francis Group.

Clauss, K., Ottinger, M., Leinenkugel, P., Kuenzer, C., 2018. Estimating rice production in the Mekong Delta, Vietnam, utilizing time series of Sentinel-1 SAR data. Int. J. Appl. Earth Obs. Geoinf. 73, 574–585. http://dx.doi.org/10.1016/j.jag.2018.07.022.

de Abelleyra, D., Iturralde Elortegui, M.d.R., Zelaya, K., Portillo, J., Melilli, M., Franzoni, A., Volante, J., Goytia, Y., Kurtz, D., Ybarra, D., Barrios, R., Benedetti, P., Morales, C., Berriolo, J., Lanceta Pereyra, M., Scavone, A., Murray, F., Santillan, J., Continelli, M., Gerlero, G., Salas, D., Reinaldi, J., Lopez Juane, P., Gomez, D., Krapovickas, S., Sapino, V., Regonat, A., Cracogna, M., Espíndola, C., Valiente, S., Parodi, M., Colombo, F., Scarel, J., Ayala, J., Martins, L., Basanta, M., Rausch, A., Almada, G., Boero, L., Calcha, J., Chiavassa, A., Calandroni, M., Murillo, M., Pascale, B., Borrachi, S., Erreguerena, J., Besteiro, I., Oyesqui, L., Lazaeta, M., Pezzola, A., Winschel, C., Rodriguez Pérez, J., German, A., Viatale, J., 2024. Argentina National Map of Crops 2023/2024. Zenodo, http://dx.doi.org/10.5281/ZENODO.13984185.

de Castro, A.L., Duarte, M.L., Ewbank, H., Lourenço, R.W., 2024. Use of synthetic aperture radar data for the determination of normalized difference vegetation index and normalized difference water index. J. Appl. Remote. Sens. 18 (1), http://dx.doi.org/10.1117/1.jrs.18.014516.

Dirección de Estimaciones Agrícolas, 2023. Datos Bioeconomía - Agricultura - Estimaciones agrícolas. URL https://datos.magyp.gob.ar/dataset/estimaciones-agricolas.

Fieuzal, R., Baup, F., 2016. Estimation of leaf area index and crop height of sunflowers using multi-temporal optical and SAR satellite data. Int. J. Remote Sens. 37 (12), 2780–2809. http://dx.doi.org/10.1080/01431161.2016.1176276.

Filgueiras, R., Mantovani, E.C., Althoff, D., Filho, E.I.F., da Cunha, F.F., 2019. Crop NDVI monitoring based on Sentinel 1. Remote. Sens. 11 (12), http://dx.doi.org/10.3390/rs11121441.

Flores, A., Herndon, K., Thapa, R., Cherrington, E., 2019. Synthetic Aperture Radar (SAR) Handbook: Comprehensive Methodologies for Forest Monitoring and Biomass Estimation. NASA, http://dx.doi.org/10.25966/NR2C-S697.

Fontanelli, G., Paloscia, S., Zribi, M., Chahbi, A., 2013. Sensitivity analysis of X-band SAR to wheat and barley leaf area index in the Merguellil Basin. Remote. Sens. Lett. 4 (11), 1107–1116. http://dx.doi.org/10.1080/2150704x.2013.842285.

Held, A., Zhou, Z.-S., Ticehurst, C., Rosenqvist, A., Parker, A., Brindle, L., 2019. Advancing Australia's imaging radar capability under the Novasar-1 partnership. In: Proceedings of IEEE International Geoscience and Remote Sensing Symposium. pp. 8370–8373. http://dx.doi.org/10.1109/IGARSS.2019.8898623.

Hirooka, Y., Homma, K., Maki, M., Sekiguchi, K., 2015. Applicability of synthetic aperture radar (SAR) to evaluate leaf area index (LAI) and its growth rate of rice in farmers' fields in Lao PDR. Field Crop. Res. 176, 119–122. http://dx.doi.org/10.1016/j.fcr.2015.02.022.

Holtgrave, A.-K., Röder, N., Ackermann, A., Erasmi, S., Kleinschmit, B., 2020. Comparing Sentinel-1 and -2 data and indices for agricultural land use monitoring. Remote. Sens. 12 (18), http://dx.doi.org/10.3390/rs12182919.

Hosseini, M., McNairn, H., 2017. Using multi-polarization C- and L-band synthetic aperture radar to estimate biomass and soil moisture of wheat fields. Int. J. Appl. Earth Obs. Geoinf. 58, 50–64. http://dx.doi.org/10.1016/j.jag.2017.01.006.

Hosseini, M., McNairn, H., Mitchell, S., Robertson, L.D., Davidson, A., Homayouni, S., 2019. Synthetic aperture radar and optical satellite data for estimating the biomass of corn. Int. J. Appl. Earth Obs. Geoinf. 83, http://dx.doi.org/10.1016/j.jag.2019.101933.

Inoue, Y., Kurosu, T., Maeno, H., Uratsuka, S., Kozu, T., Dabrowska-Zielinska, K., Qi, J., 2002. Season-long daily measurements of multifrequency (Ka, Ku, X, C, and L) and full-polarization backscatter signatures over paddy rice field and their relationship with biological variables. Remote Sens. Environ. 81 (2–3), 194–204. http://dx.doi.org/10.1016/s0034-4257(01)00343-1.

Jia, M., Tong, L., Zhang, Y., Chen, Y., Chopra, R., 2014. Multi-temporal radar backscattering measurements and modelling of rice fields using a multi-frequency (L, S, C, and X) scatterometer. Int. J. Remote Sens. 35 (4), 1253–1271. http://dx.doi.org/10.1080/01431161.2013.876117.

Jiao, X., McNairn, H., Robertson, L.D., 2021. Monitoring crop growth using a canopy structure dynamic model and time series of synthetic aperture radar (SAR) data. Int. J. Remote Sens. 42 (17), 6433–6460. http://dx.doi.org/10.1080/01431161.2021.1938739.

Joshi, A., Agrawal, S., Chauhan, P., 2022. Geolocation accuracy improvement for NovaSAR-1 imagery acquired through TLE orbit. Geocarto Int. 37 (26), 12414–12435. http://dx.doi.org/10.1080/10106049.2022.2066727.

Karger, D.N., Conrad, O., Böhner, J., Kawohl, T., Kreft, H., Soria-Auza, R.W., Zimmermann, N.E., Linder, H.P., Kessler, M., 2017. Climatologies at high resolution for the earth's land surface areas. Sci. Data 4 (1), http://dx.doi.org/10.1038/sdata.2017.122.

Karger, D.N., Conrad, O., Böhner, J., Kawohl, T., Kreft, H., Soria-Auza, R.W., Zimmermann, N.E., Linder, H.P., Kessler, M., 2021. CHELSA. http://dx.doi.org/10.16904/ENVIDAT.228.V2.1.

Kim, Y., Lee, H., Hong, S., 2013. Continuous monitoring of rice growth with a stable ground-based scatterometer system. IEEE Geosci. Remote. Sens. Lett. 10 (4), 831–835. http://dx.doi.org/10.1109/lgrs.2012.2225595.

Kim, Y., van Zyl, J., 2000. On the relationship between polarimetric parameters. In: Proceedings of IEEE International Geoscience and Remote Sensing Symposium, vol. 3. IEEE, pp. 1298–1300. http://dx.doi.org/10.1109/igarss.2000.858099.

Li, Y., Chen, X., Chen, Z., Hu, C., 2022. S-band spaceborne SAR interferometric coherence analysis: A study case in Peth, Australia. In: Proceedings of IEEE International Geoscience and Remote Sensing Symposium. pp. 5812–5815. http://dx.doi.org/10.1109/igarss46834.2022.9883695.

Liao, C., Wang, J., Shang, J., Huang, X., Liu, J., Huffman, T., 2017. Sensitivity study of Radarsat-2 polarimetric SAR to crop height and fractional vegetation cover of corn and wheat. Int. J. Remote Sens. 39 (5), 1475–1490. http://dx.doi.org/10.1080/01431161.2017.1407046.

Lopez-Sanchez, J.M., Vicente-Guijalba, F., Ballester-Berman, J.D., Cloude, S.R., 2014. Polarimetric response of rice fields at C-band: Analysis and phenology retrieval. IEEE Trans. Geosci. Remote Sens. 52 (5), 2977–2993. http://dx.doi.org/10.1109/tgrs.2013.2268319.

Macelloni, G., Paloscia, S., Pampaloni, P., Marliani, F., Gai, M., 2001. The relationship between the backscattering coefficient and the biomass of narrow and broad leaf crops. IEEE Trans. Geosci. Remote Sens. 39 (4), 873–884. http://dx.doi.org/10.1109/36.917914.

Nasirzadehdizaji, R., Balik Sanli, F., Abdikan, S., Cakir, Z., Sekertekin, A., Ustuner, M., 2019. Sensitivity analysis of multi-temporal Sentinel-1 SAR parameters to crop height and canopy coverage. Appl. Sci. 9 (4), http://dx.doi.org/10.3390/app9040655.

Oh, Y., Hong, S.-Y., Kim, Y., Hong, J.-Y., Kim, Y.-H., 2009. Polarimetric backscattering coefficients of flooded rice fields at L- and C-Bands: Measurements, modeling, and data analysis. IEEE Trans. Geosci. Remote Sens. 47 (8), 2714–2721. http://dx.doi.org/10.1109/tgrs.2009.2014053.

Onojeghuo, A.O., Blackburn, G.A., Wang, Q., Atkinson, P.M., Kindred, D., Miao, Y., 2018. Rice crop phenology mapping at high spatial and temporal resolution using downscaled MODIS time-series. GIScience & Remote. Sens. 55 (5), 659–677. http://dx.doi.org/10.1080/15481603.2018.1423725.

Paloscia, S., 2002. A summary of experimental results to assess the contribution of SAR for mapping vegetation biomass and soil moisture. Can. J. Remote Sens. 28 (2), 246–261. http://dx.doi.org/10.5589/m02-020.

Pandit, A., Sawant, S., Mohite, J., Rajpoot, N., Pappula, S., 2023. Can radar backscatter ratio be used to estimate NDVI and act as its substitute? – A study over winter wheat crop in India. ISPRS Ann. Photogramm. Remote. Sens. Spat. Inf. Sci. X-1/W1-2023, 857–862. http://dx.doi.org/10.5194/isprs-annals-x-1-w1-2023-857-2023.

Roa, Y., Rosell, P., Solarte, A., Euillades, L., Carballo, F., García, S., Euillades, P., 2021. First assessment of the interferometric capabilities of SAOCOM-1A: New results over the Domuyo Volcano, Neuquén Argentina. J. South Am. Earth Sci. 106, http://dx.doi.org/10.1016/j.jsames.2020.102882.

Rosenqvist, A., Killough, B., 2018. A Layman's Interpretation Guide to L-band and C-band Synthetic Aperture Radar data. URL https://ceos.org/ard/files/Laymans_SAR_Interpretation_Guide_2.0.pdf,

Roßberg, T., Schmitt, M., 2023. A globally applicable method for NDVI estimation from Sentinel-1 SAR backscatter using a deep neural network and the SEN12TP dataset. J. Photogramm. Remote. Sens. Geoinf. Sci. 91, 171–188. http://dx.doi.org/10.1007/s41064-023-00238-y.

Roßberg, T., Schmitt, M., 2024. Comparing SAR at multiple frequencies with optical vegetation indices for an area in Vietnam. In: Proceedings of 15th European Conference on Synthetic Aperture Radar. pp. 650–653.

Roßberg, T., Schmitt, M., 2025. Acompanying data for "Comparing the relationship between NDVI and SAR backscatter across different frequency bands in agricultural areas", version 1. Open Data UniBw M, http://dx.doi.org/10.60776/4WIAJ0.

dos Santos, E.P., da Silva, D.D., do Amaral, C.H., Fernandes-Filho, E.I., Dias, R.L.S., 2022. A machine learning approach to reconstruct cloudy affected vegetation indices imagery via data fusion from Sentinel-1 and Landsat 8. Comput. Electron. Agric. 194, http://dx.doi.org/10.1016/j.compag.2022.106753.

Scarpa, G., Gargiulo, M., Mazza, A., Gaetano, R., 2018. A CNN-based fusion method for feature extraction from Sentinel data. Remote. Sens. 10 (2), http://dx.doi.org/10.3390/rs10020236.

Segalini, F., Guarini, R., Notarnicola, C., Vuolo, F., Dini, L., 2014. COSMO-SkyMed® imagery for crops characterization. In: Proceedings of 34th EARSeL Symposium. pp. 7.1–7.11. http://dx.doi.org/10.12760/03-2014-17.

Torres, R., Snoeij, P., Geudtner, D., Bibby, D., Davidson, M., Attema, E., Potin, P., Rommen, B., Floury, N., Brown, M., Traver, I.N., Deghaye, P., Duesmann, B., Rosich, B., Miranda, N., Bruno, C., L'Abbate, M., Croci, R., Pietropaolo, A., Huchler, M., Rostan, F., 2012. GMES Sentinel-1 mission. Remote. Sens. Environ. 120, 9–24. http://dx.doi.org/10.1016/j.rse.2011.05.028.

Trudel, M., Charbonneau, F., Leconte, R., 2012. Using RADARSAT-2 polarimetric and ENVISAT-ASAR dual-polarization data for estimating soil moisture over agricultural fields. Can. J. Remote Sens. 38 (4), 514–527. http://dx.doi.org/10.5589/m12-043.

Truong, V.T., Hirayama, S., Phan, D.C., Hoang, T.T., Tadono, T., Nasahara, K.N., 2024. JAXA's new high-resolution land use land cover map for Vietnam using a time-feature convolutional neural network. Sci. Rep. 14, http://dx.doi.org/10.1038/s41598-024-54308-1.

U.S. Department of Agriculture, Foreign Agricultural Service, International Production Assessment Division, 2017. South east Asia - crop production maps. URL https://ipad.fas.usda.gov/rssiws/al/crop_production_maps/seasia/Vietnam_Total_Rice.png.

U.S. Department of Agriculture, Foreign Agricultural Service, International Production Assessment Division, 2021. Crop calendars for Australia. URL https://ipad.fas.usda.gov/rssiws/al/crop_calendar/as.aspx.

Villarroya-Carpio, A., Lopez-Sanchez, J.M., 2023. Multi-annual evaluation of time series of Sentinel-1 interferometric coherence as a tool for crop monitoring. Sensors 23 (4), http://dx.doi.org/10.3390/s23041833.

Villarroya-Carpio, A., Lopez-Sanchez, J.M., 2024. Influence of temporal baseline on X-band repeat-pass coherence for crop monitoring. In: Proceedings of 15th European Conference on Synthetic Aperture Radar. pp. 678–683.

Villarroya-Carpio, A., Lopez-Sanchez, J.M., Engdahl, M.E., 2022. Sentinel-1 interferometric coherence as a vegetation index for agriculture. Remote. Sens. Environ. 280, http://dx.doi.org/10.1016/j.rse.2022.113208.

Wang, X., Ge, L., Li, X., 2013. Pasture monitoring using SAR with COSMO-SkyMed, ENVISAT ASAR, and ALOS PALSAR in Otway, Australia. Remote. Sens. 5 (7), 3611–3636. http://dx.doi.org/10.3390/rs5073611.

Weiss, M., Jacob, F., Duveiller, G., 2020. Remote sensing for agricultural applications: A meta-review. Remote. Sens. Environ. 236, http://dx.doi.org/10.1016/j.rse.2019.111402.

Xu, H., 2006. Modification of normalised difference water index (NDWI) to enhance open water features in remotely sensed imagery. Int. J. Remote Sens. 27 (14), 3025–3033. http://dx.doi.org/10.1080/01431160600589179.

Zhang, J., Huang, Y., Pu, R., Gonzalez-Moreno, P., Yuan, L., Wu, K., Huang, W., 2019. Monitoring plant diseases and pests through remote sensing technology: A review. Comput. Electron. Agric. 165, 104943. http://dx.doi.org/10.1016/j.compag.2019.104943.

Zhou, X., Zheng, H.B., Xu, X.Q., He, J.Y., Ge, X.K., Yao, X., Cheng, T., Zhu, Y., Cao, W.X., Tian, Y.C., 2017. Predicting grain yield in rice using multi-temporal vegetation indices from UAV-based multispectral and digital imagery. ISPRS J. Photogramm. Remote. Sens. 130, 246–255. http://dx.doi.org/10.1016/j.isprsjprs.2017.05.003.